

THESIS FOR DEGREE OF DOCTOR OF PHILOSOPHY

Ion Conduction and the Bond Valence Method in Glasses

ANDREAS J. HALL



Department of Applied Physics
CHALMERS UNIVERSITY OF TECHNOLOGY
Göteborg, Sweden 2008

Ion Conduction and the Bond Valence Method in Glasses

ANDREAS J. HALL

ISBN 978-91-7385-219-7

Doktorsavhandlingar vid Chalmers tekniska högskola, Ny serie nr 2900.

ISSN 0346-718X.

© Andreas J. Hall, 2008, unless otherwise stated.

Department of Applied Physics
Chalmers University of Technology
SE-412 96 Göteborg
Sweden
Telephone +46 (0)31-772 1000

Cover picture:

Rendition of the Ag (yellow) Na (blue) and common (magenta) ionic pathways in $\text{Ag}_{0.5}\text{Na}_{0.5}\text{PO}_3$ with a random transparency to emphasize their similarities. Further details given in paper V.

Also showing; a rabbit with yellow leafs on its feet (far left).

Chalmers reproservice
Göteborg, Sweden 2008

Ion Conduction and the Bond Valence Method in Glasses

ANDREAS HALL

Department of Applied Physics

Chalmers University of Technology

ABSTRACT

Ion conducting glasses are highly interesting for several different applications, among them, chemical sensors, smart windows with variable optical properties and as electrolytes in batteries. The last example can take full advantage of the ease with which a thin film ($< 1\mu\text{m}$) of glass electrolyte can be sputtered onto a substrate and thereby provide power for micro-scale electronics, e.g., a chip on so called smart cards. However, despite intense research there is still no fully satisfactory model for the atomic mechanics governing the ion conduction in these materials. In many promising materials (e.g. nitrated phosphate films) we have not even access to good models of their structure.

The aim of this thesis is to shed some light on both the structure and ionic properties of ionic oxide glasses. The structure is determined by a combination of neutron and X-ray diffraction experiments together with the reverse Monte Carlo technique, with which we can create structural models of the investigated glasses. These structural models can then be analyzed in terms of pair correlations, topology and possible structural inhomogeneities. Furthermore, the application of the bond valence method to the structures yields vivid representations of the ionic pathways through the structures. From these, not only estimations of the activation energy and conductivity can be extracted, but also important information on coordination of mobile ions and pathway topography can be gained. These techniques have here been used for investigations of two different phenomena.

Firstly, when a network modified oxide glass, such as $\text{M}_2\text{O}-\text{B}_2\text{O}_3$, is doped by a metal halide salt, MX, a strong increase in conductivity can be seen. Earlier structural studies have shown how salt-rich channels through the oxide network is formed. Our investigations show the distinctly different pathways in differently doped systems. Furthermore, we show that ordering of the glass beyond the nearest neighbors play little role in ion conduction.

Secondly, the ever elusive mixed mobile ion effect (MMIE) has been placed under scrutiny. The strong MMIE in a mixed Li/Rb meta-phosphate has been investigated in terms of the pathway topography and the blocking effect both at room temperature and near the glass transition. A study of the weak MMIE in a Ag/Na meta-phosphate system reveals the similarities in pathways for the two types of ions. In this system we find no blocking effect and propose the existence of cooperative Ag-Na pairs in the pathways.

Keywords:

Glass structure, Ion conduction, Bond valence method, Reverse Monte Carlo, X-ray diffraction, Neutron diffraction, Phosphate glasses, Borate glasses

APPENDED PAPERS

This thesis is based on the work contained in the following papers:

I The Nature of Conduction Pathways in Mixed Alkali Phosphate glasses

A. Hall, S. Adams and J. Swenson

Ionics **10**, 396-404 (2004)

II Local dimensionality and intermediate range ordering of ion conduction pathways in borate glasses.

A. Hall, S. Adams and J. Swenson

Journal of Non-Crystalline Solids **42-49**, 5164-5169 (2006)

III Comparative study of ion conducting pathways in borate glasses

A. Hall, S. Adams and J. Swenson

Physical Review B: Condensed Matter **74**, 174205 (2006)

IV Structure of $\text{Ag}_x\text{Na}_{(1-x)}\text{PO}_3$ glasses by neutron diffraction and reverse Monte Carlo modelling

A. Hall, J. Swenson, S. Adams and D.T. Bowron

Journal of Physics: Condensed Matter **19**, 415115 (2007)

V Mixed Mobile Ion Effect and Cooperative Motions in Silver-Sodium Phosphate Glasses

A. Hall, J. Swenson, S. Adams and C. Meneghini

Physical Review Letters **101**, 195901 (2008)

VI Structure of $\text{Li}_x\text{Rb}_{(1-x)}\text{PO}_3$ Glasses Near the Glass Transition Temperature

A. Hall, J. Swenson, S. Adams and D.T. Bowron

(Manuscript)

Contents

1	INTRODUCTION	1
2	The Structure and Formation of Glasses	5
2.1	Glasses and Amorphous Materials	5
2.1.1	The Order of Disorder	8
2.1.2	Quantifying Correlations	10
2.2	Covalent Glass Models	11
2.2.1	Phosphate Glasses	13
2.2.2	Borate Glasses	14
2.2.3	Halide Salt Doping	15
3	Ionic Conduction in Solid electrolytes	17
3.1	Crystalline Ion Conductors	17
3.2	Conduction Models in Glasses	19
3.2.1	The Anderson-Stuart Model	21
3.2.2	Weak Electrolyte Model	21
3.2.3	Dynamic Models	22
3.3	Mixed Mobile Ion Effect	23
4	Experimental Probes	27
4.1	Macroscopic Scale Probes	27
4.1.1	Differential Scanning Calorimetry	28
4.2	Vibrational Spectroscopy	28
4.3	Atom Specific Probes	30
4.4	Diffraction Techniques	30
4.4.1	Neutron Diffraction	31
4.4.2	X-ray Diffraction	33
5	Structural Modeling and the Bond Valence Method	35

5.1	Modeling Amorphous Materials	35
5.1.1	Molecular Dynamics	35
5.1.2	Metropolis Monte Carlo	37
5.1.3	Reverse Monte Carlo	39
5.2	The Bond Valence Method	43
5.2.1	Bond Valence and Ionic Conductivity	45
6	Summary of Appended Papers	49
	Acknowledgments	53
	Bibliography	55

CHAPTER 1

INTRODUCTION

Glasses are by no means new materials, they have been around on earth since it was cool enough for the formation of the crust. One common natural source of glasses are meteorite impacts, large enough to melt the sand and rock, which form glass as it cools down. Large fields of strewn natural glass are many times linked to known or speculated impact sites, e.g., the Tektite fields in Argentinean Pampa (1) and the Dakhleh glass in western Egypt (2). Another source is volcanic eruptions in which obsidian can form as the molten rock rapidly cools in the air. This hard, glassy material, which form sharp edges when broken, has been used in stone age for various cutting tools. Interestingly, obsidian is still used in modern surgical scalpels (3; 4). Man made glasses started to appear in the region of modern Egypt, at least 9000 years ago. First admired for their beauty and used for decorative purposes, but with time the skill of glass making grew and with new recipes and shaping techniques, the uses of glasses diverged. However, when it comes to structural knowledge of glasses, very little was know until powerful experimental techniques were developed in the beginning of the last century.

Due to their simple structure, crystalline solids were generally the first to be studied by these new techniques for structural characterization. Their static structure have been investigated by predominately X-ray but also neutron diffraction. Their ideal structure (where all atoms are located in their equilibrium position) can be constructed in terms of crystalline unit cells, typically comprising of 1-10 atoms for simple ionic or metallic materials. Their dynamical properties and vibrational modes can likewise be studied by means of, e.g., inelastic neutron diffraction or IR/Raman and later modeled using the same simple crystalline unit cell. Since the crystalline structure is well understood, the ionic conduction process in these materials can often be classified as being either of point defect or molten sublattice type (cf. chapter 3)

In glasses and other amorphous materials on the other hand we have, despite

intense investigations, not yet reached the same level of understanding as of the crystalline state. Partially this is due to the inherent disorder of the materials which breaks the symmetries of the crystal state that make its description so easy. A large part of the vocabulary developed in crystallography (e.g. interstitial, vacancy, reciprocal lattice, crystal defects) to describe the structure and its properties have little or no meaning when applied to amorphous materials, whereas some terminology (e.g. inter-atomic distance, coordination number) may be given a slightly broader definition and still have a place in the description of the glassy state. Similarly, the ionic transport can not be described in the crystallographic terminology since terms as vacancy and interstitiality no longer have a well defined meaning.

The problems of classifying amorphous materials and their properties also stem from the problem of creating realistic structural models of the glassy state. Instead of creating an ideal structure as can be done for crystals, we have to create structural models that can reproduce as many of the properties of the glass as possible. In the early days of glass science, models were of a conceptual kind and were mostly based on the chemical knowledge of preferences of bonds made by the atoms in the glass. Among the more successful models are the *continuous random network model* introduced 1933 (5) that to this day is used to describe the structure of network forming glasses, and the *dense random packing of hard spheres* model which describes ionic and metallic glasses quite well. These kinds of simple models capture the essential structural features of glasses, but cannot fully account for advanced properties such as vibrations, relaxations and diffusion.

With the advances made in microelectronics, computer models have become a valuable tool for modeling both static structures as well as dynamics in complex molecular systems. With techniques such as molecular dynamics (MD) simulation and reverse Monte Carlo (RMC) modeling (cf. section 5.1), quantitative models of glasses that reproduce many of the experimentally observed features may be constructed. With MD simulation, microscopic processes such as ionic transport and structural relaxation can be studied in greater detail than what most experimental techniques allow (due to their space and time averaging). Furthermore, one can study the detailed movement of a single ion through, e.g., a glass and thereby investigate details of the conduction pathways and equilibrium sites of the ion, but the simulations can only follow the ion over a limited period of time, and for disordered systems, important features of conduction pathways may be overlooked.

In this thesis, we instead try to classify the conduction pathways in glasses starting from a static structure model (here modeled by the RMC method, cf. section 5.1.3 and calculate the pathways by means of bond valence pseudo potential calculations (BV, cf. 5.2, a method that previously has proved to be a valuable tool in structure determinations. The advantage of pathway calculations by the BV method over MD is that from BV, all possible diffusion pathways are found, rather than only those who are visited by an ion in the MD approach. The pathways give a vivid picture of where the ionic transport occurs in the glass. From the volume of the pathways, estimations of the ionic dc conductivity and activation energy can be made, and detailed studies of the pathways have given further insight into various aspects

of ionic conduction. For instance, the so-called mixed mobile ion effect the relation between intermediate range order and conductivity in salt doped glasses have been explored.

The Structure and Formation of Glasses

2.1 Glasses and Amorphous Materials

Although the term 'glass' is often used to refer to silicate based glasses, its true meaning is much broader than this. There are several definitions of a glass, but here we will adhere to the definition given in ref. (6)

A glass is an amorphous solid which exhibits a glass transition

Now we need to define amorphous, solid and glass transition, but before doing that it can be illustrative to make a brief review of another phase of matter; the crystalline state. Most crystalline materials are quite well understood due to their relatively simple structure. The atomic arrangement in crystals is described in terms of a crystallographic lattice, i.e. a distribution of points (lattice point) in space such that every point has an identical surrounding. The set of lattice points can be described by

$$\mathbf{r} = n_1 \mathbf{a}_1 + n_2 \mathbf{a}_2 + n_3 \mathbf{a}_3, \quad (2.1)$$

where n_i are integers and \mathbf{a}_i are the basis vectors of the lattice.

There is a total of 14 different regular arrangements of identical points that fill 3d space and these are called the Bravais lattices. Most crystals however contain more than one type of atom, and their positions can be described by associating each point of the correct Bravais lattice with a set of j atoms, a so called basis, \mathbf{R}_j . The atomic positions are then

$$\mathbf{r} = n_1 \mathbf{a}_1 + n_2 \mathbf{a}_2 + n_3 \mathbf{a}_3 + \mathbf{R}_j, \quad (2.2)$$

where \mathbf{R}_j is the position of atom j in the basis, relative to the lattice point. This gives us a complete description of the atomic arrangement in an ideal crystal, and since all

lattice points are symmetrically identical, the volume spanned by the basis vectors is sufficient to give a complete description of the crystal, although one often chooses a slightly larger unit cell of convenience. In reality though, the actual positions of atoms differs slightly from their ideal due to thermal vibrations and crystal defects (vacancies, substitutions etc.) but these deviations from the ideal case can often be neglected.

The perfect translational symmetry in the ideal crystal, where identical unit cells are repeated ad infinitum also implies that all crystals have discrete rotational symmetry. This anisotropy can be readily seen in macroscopic samples. Since the velocity of light traveling through a crystal depends on its direction, crystalline materials are not suitable for e.g. optical lenses, and when crystals break, they usually do so along specific directions - along the lattice planes. And this anisotropy can also extend to e.g. ionic transport. Many crystals have preferred directions of ionic diffusion with pathways that sometimes are 2 or even 1 dimensional.

When a crystal is heated each atom will be given a higher vibrational energy and at a specific temperature, the melting temperature T_m , the thermal energy is large enough to break (some of) the bonds in the crystal. Since all unit cells are equivalent, this bond breaking would for a perfect heating occur simultaneously in all equivalent bonds, and the transition between solid and liquid is marked by a discontinuity in observable quantities such as viscosity, molar volume and entropy. Thermodynamically, this is a so called first order transition.

Now that we know what a crystal is, we can turn our attention to the amorphous state as it is easiest defined as being 'not crystalline'. This group of materials lack the long range order that crystalline materials possess, and are thus impossible to describe in terms of simple unit cells. It is however worth noticing that these materials still have some degree of ordering, on short length scales even a considerable amount, as we will see in the next section.

Solid has a rather intuitive definition to most of us. In a macroscopic perspective, we may define a solid material as a material that does not flow under stress. While moderate forces acting on a sample will deform it, the deformation is reversible and the sample will return to its original form once the forces are removed. We know however that many solids may change their form if the acting forces are strong enough, but the deformations are not due to flow, but *creep*, a process where the bonds within the material are broken and reformed in new configurations. Allowing even stronger forces, we will ultimately break the solid into fragments. On an atomic scale, however, it is somewhat more difficult to separate the solid state from the liquid. In the case of crystalline materials, we have a distinct, 1st order thermodynamical transition between the liquid state and the solid crystalline state. The liquid is composed of atoms, ions or molecules that are loosely bonded to each other. Bonds between these units are broken and formed continuously in time and although structures of several molecules may form, they are rarely stable for any extended period of time, e.g., heterogeneity in water (7). In crystals on the other hand, all atoms are in fixed positions and bond breaking is very rare. In other cases, the distinction between liquid and solid is not as clear. Liquid crystals are in a con-

densed state that poses long range order, like the crystalline state, yet many of them have flow properties similar to those of liquids. Furthermore, upon cooling many of them exhibit more than one liquid crystalline state before they freeze to a solid (cf. (8)).

Yet another example is pitch. In room temperature most of us would mistake pitch for a solid; it resists moderate forces and shatters if struck by e.g. a hammer, but is in fact a liquid of high viscosity as is demonstrated in the pitch drop experiment [6, 7] where pitch is slowly dropping out from a glass funnel. In the past 76 years, 8 drops have fallen so far. For this reason, solids are also commonly defined by the somewhat arbitrary requirement that they should have a shear viscosity of at least $10^{13.6}$ Pa s.

The final criterion for a glass is that it exhibits a glass transition. When a melt is cooled, the viscosity of the liquid increases since the lower temperature allows more stable (although still temporary) bonds to form between atoms, ions or molecules. If the cooling is slow compared to the timescale of structural relaxations in the liquid (proportional to the viscosity), a nucleation and growth process can create a crystalline structure at the melting point (T_m). However if the cooling is rapid, we may supercool the liquid. When the viscosity becomes high enough, the liquid cannot relax to the energetically favorable crystalline state and is thus trapped in a liquid like state. As temperature is lowered further, viscosity increases and eventually the melt will go through the glass transition and form a glass. The glass transition is characterized by a near discontinuity, e.g., in the heat capacity (C_p) and thermal expansion coefficient (κ) as showed in figure 2.1, while other quantities such as molar volume (plotted against temperature) experiences a change of slope. The exact definition of the glass transition temperature (T_g) varies somewhat, but one common definition is to set T_g at the center of the discontinuity. The exact nature of the glass transition is

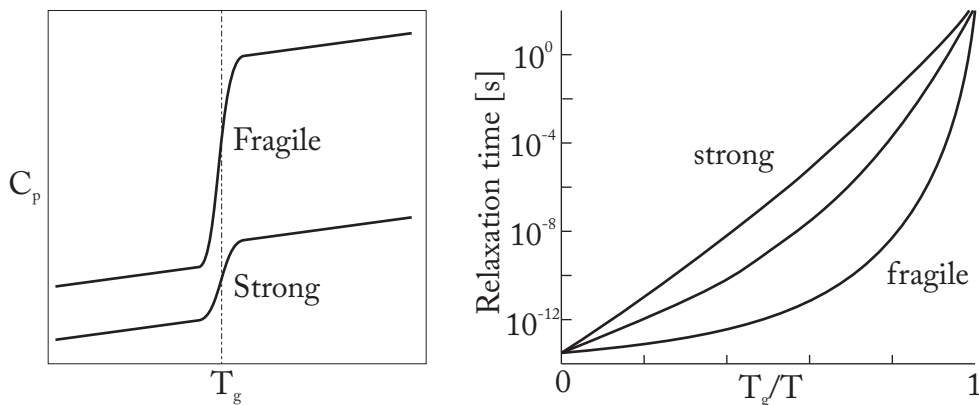


Figure 2.1: Change in C_p at T_g for two different glass formers. Cf. figure 4.1(left) and the temperature–relaxation time relation for three glass formers of different *fragility*. The fragility of a supercooled liquid depends strongly on the bonding strength between atoms and/or molecules in the material. A *strong* liquids exhibit an Arrhenius temperature dependence of the structural relaxation time (or viscosity), whereas a fragile liquid exhibits a pronounced non-Arrhenius behavior.

however not fully understood. The perhaps most commonly accepted model is the kinetic theory outlined above, but there are several other models that each focus on different aspects of the transition. As a melt cools into a glass, extensive thermodynamical variables such as volume, entropy and enthalpy are continuous through the transition, unlike in the first order liquid-crystal transition where they are discontinuous at the melting point. The derivatives of these quantities (heat capacity, thermal expansion coefficient etc.) are however nearly discontinuous, suggesting that the glass transition is in fact a second order thermodynamical transition. However this is contradicted by the fact that the glass transition temperature depends on the history of the glass, such as the cooling rate. Arguments based on entropy suggest that there is an 'ideal' glass transition temperature. At this hypothetical transition temperature, the liquid would have the same configurational entropy as the corresponding crystalline state.

So, what substances form a glass phase when cooled? A glass is formed if the cooling rate is fast compared to the rate of nucleation. Hence, liquids which easily crystallize, such as water, have to be very rapidly cooled below their melting temperatures to prevent crystallization, whereas other liquids, such as B_2O_3 , are, in fact, difficult to crystallize and are therefore easily cooled down to the glassy state. Indeed, it has been hypothesized that all substances that can form a solid, can also be produced in glass phase, given high enough cooling rate.

2.1.1 The Order of Disorder

Let us now take a closer look at how glasses are structured on an atomic level. Glasses and other amorphous materials are defined by their lack of long range order, but that is not to say that they completely lack ordered structure. On the contrary some glasses, in particular covalently bonded glasses can have a significant amount of order on length scales of up to 20 \AA , and density fluctuations in the material can be relevant on even longer length scales. Here we will take a closer look at what order we do have in glasses and where the disorder comes in.

On the shortest length scale we have the order among nearest neighbor atoms in the glass. This range of order is called the short range order (SRO) and thus contains information on the distances and relative angles to the nearest neighbors of any atom, as well as the chemical specie of these neighbors. The SRO in glasses is highly dependent on the kind of glass we are discussing. Metallic and ionic glasses are composed of atoms bond together by mainly non-directional forces. In ionic metals, Coulomb forces between the differently charged ions binds the atoms to each other and in metallic glasses the attractive potential comes from the sharing of their valence electrons. The distribution of atoms in these two types of glasses can be described rather well by a dense random packing of spheres model (DRPS)(9) and the SRO present in these glasses thus only determines the nearest neighbor distances between atoms. In covalent glasses there is more to the SRO than nearest neighbor distances. Covalent bonds are highly directional and the distances and angles between anions coordinating to a single cation are in general very well defined.

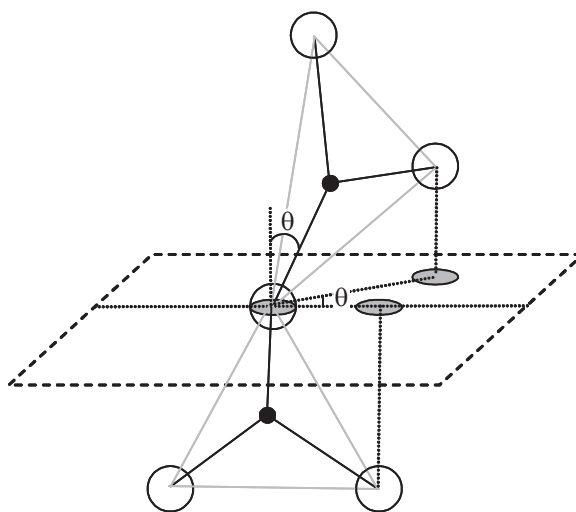


Figure 2.2: Depiction of bond distortion between two planar, corner-sharing polyhedra, showing bond angle (θ) and rotational (ϕ) distortions. ©D. Staykova.

The basic building blocks in these glasses are thus basically the same as in the corresponding crystalline phases, i.e. coordination polyhedra with a cation in the center and anions located at the corners, see section 2.2.

The intermediate range order (IRO) stretches over the range of ca 5-20 Å and describes for instance the connectivity between covalent polyhedra, are they corner, edge or even face-sharing, and what is the bond angle between them? While the length of the bonds in general is well defined due to relatively large changes in bond energy with bond length, distortions in the bond angles (θ) and rotational distortions (ϕ) (see figure 2.2) require less energy and is thus more frequent. These distortions of the connections of polyhedra yield a structure that differs from the corresponding crystal, and thus the disorder in covalent glasses is created.

IRO may also arise from superstructural units of several coordination polyhedra, such as rings or clusters. An example of such superstructural units is the boroxol ring which is a part of the vitreous B_2O_3 structure [9]. Other types of correlations may emerge from relatively well-defined distance between different chains of coordination polyhedra. Such correlations are obvious in e.g. Ag_2O modified borate glasses where the metal ions create a typical distance of 5 Å between neighboring borate chains, an order that can be observed for length-scales up to 10-20 Å (see papers II and III and references therein).

At even greater length scales > 20 Å we enter the long range order (LRO) in which few glasses show any features. Still, some glasses may exhibit weak density fluctuations that may be of interest to characterize. In particular, possible clustering of, e.g., metal ions may occur on these length scales.

2.1.2 Quantifying Correlations

Glasses and other amorphous materials can, as we have seen, not be described in the simple unit cell scheme that has proven useful for crystalline materials. Instead, we may describe the order in the material by means of correlation functions.

The density function, $\rho(\mathbf{r})$, is defined such that given that there is an atom at $\mathbf{r} = \mathbf{0}$, then the number of atoms within the small volume ΔV around the position \mathbf{R} is expected to be $\Delta V \rho(\mathbf{R})$. This implies that

$$\iiint_{\text{sample}} d\mathbf{r} \rho(\mathbf{r}) = N, \quad (2.3)$$

where N is the total number of atoms in the sample.

Note that $\rho(\mathbf{r})$ is an average over all atoms in the system. Since we are here interested in describing an isotropic system where each atom has a unique surrounding in terms of coordination and orientations, $\rho(\mathbf{r})$ is spherically symmetrical and we may drop the vector notation altogether and concern ourselves with $\rho(r)$, where $r = |\mathbf{r}|$, a function of distance alone.

At radii below the shortest nearest neighbor distance $\rho(r) \equiv 0$ since no correlations exist at these distances. At larger radii, $\rho(r)$ exhibits an oscillatory behavior that, in amorphous materials and liquids, is dampened with increasing radius and approaches the average density, ρ_0 .

Other correlation functions can be derived from the density function, such as the radial distribution function (RDF), defined as

$$J(r) = 4\pi r^2 \rho(r), \quad (2.4)$$

and the reduced radial distribution function (rRDF),

$$G(r) = 4\pi r(\rho(r) - \rho_0). \quad (2.5)$$

$J(r)$ increases rapidly for large r values, but is useful in the investigation of nearest and next-nearest neighbor coordination shells since an integration over the peak directly gives the number of atoms in that coordination shell. $G(r)$ on the other hand oscillates around zero, but the linear r -term amplifies small peaks at higher radii, making them easier to discern than from the density function directly. Furthermore, the rRDF is often used in neutron and X-ray discussions since it is related to the structure factor $S(Q)$, a correlation function in reciprocal space (cf. section 4.4.1).

These correlation functions also exist in atom-specific forms, such as the partial density function $\rho_{ij}(r)$ which is defined such that given that there is an atom of type i at $r = 0$, then $\Delta V \rho_{ij}(R)$ is the average number of atoms of type j within the volume ΔV at distance R . Correspondingly, the partial RDF, $J_{ij}(r)$, and partial rRDF $G_{ij}(r)$ can be defined by insertion of $\rho_{ij}(r)$ into equations 2.4 and 2.5.

2.2 Covalent Glass Models

Covalently bonded glasses are an important group. The basic structure is that of a well defined coordination tetrahedron where a central cation is coordinated to surrounding anion. Covalent bonds are strong and highly directional meaning that the tetrahedra are only slightly distorted by addition of different modifiers and/or glass preparations. Additionally, in the unmodified glasses, each tetrahedron shares at least three of its anions, thereby not only creating a strong network, but also a high viscous melt which make them excellent glass formers. Here, we will look at two conceptual models for this glass type and compare the models to the experimentally verified structures of phosphate and borate glasses.

Conceptual structure models are simple qualitative descriptions that aim to explain some of the features of real glass samples. Though many of them can be explained using only a few sentences, they can be surprisingly accurate in their predictions of at least parts of the glass behavior. Here, we will discuss the structure of covalent glasses from the standpoint of two such models, the continuous random network model (CRN), that describes covalently bonded glasses on the form A_xB_y ($A=B,P,Si,W,\dots$; $B=O,S,F,\dots$), and the modified continuous random network model (MRN), which addresses glasses that have been network modified by metal oxide. Both of the models give a vivid picture of the glass structure that (with minor modifications) is still valid today. We will also discuss how the structure is affected by the introduction of additional metal halide salts.

One of the perhaps most fundamental papers in structural glass science was written by Zachariasen in 1932 (5), where he presented what would later be known as the continuous random network model of covalent oxide glasses of type $A_xO_y^*$. At the time, many assumed that the atomic arrangement of glasses would follow the microcrystalline model, or the related crystallite model, according to which the atoms were arranged in nano-scale crystal-like structures (≈ 15 nm in diameter), with an amorphous grain boundary as their interfaces. This model, however, does not agree well with several experimental observations. Zachariasen argued that the forces keeping the structure together in a glass should be similar to those in the corresponding crystal, and that the glass should be built up of a 3d network similar to that found in crystals, but lacking their periodicity. Studying the topology, Zachariasen concluded that for a glass (covalent oxide glass) with an energy comparable to that of the crystalline state, four rules should be met:

1. An oxygen is linked to not more than two atoms
2. The number of atoms surrounding atom A must be small
3. The oxygen polyhedra share corners with each other, not edges or faces
4. At least three corners in each oxygen polyhedra must be shared.

*The less common sulphide glasses, A_xS_y have a similar structure and can also be described by the CRN model

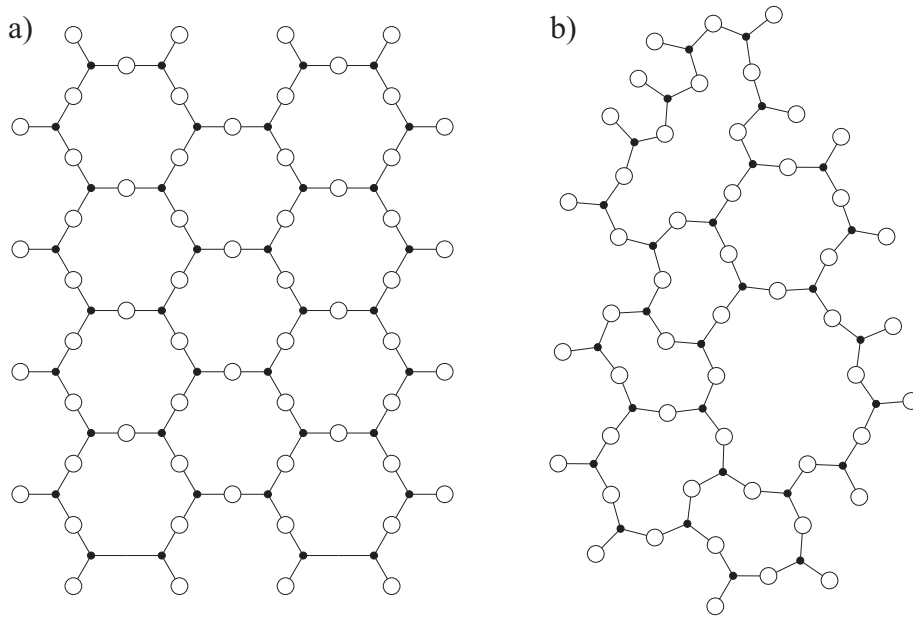


Figure 2.3: A 2-dimensional A_2O_3 crystal on the left, and on the right the corresponding CRN model

Due to the absence of crystalline materials with a octagonal or cubic oxygen polyhedron that can be easily prepared in a vitreous state, Zachariasen concluded that rule 2 thus only allows triangular and tetrahedral coordination polyhedra.

Figure 2.3 shows a 2d representation of a A_2O_3 compound in a) its crystalline state and b) its glassy state according to the CRN model. In both cases all the bonds are of the same type and there are no dangling bonds in the structure, the difference is the slight distortions of bond angles that break the translational symmetry in the glassy state. The model predicts correctly that oxides of types A_2O_3 (provided that the oxygens form triangles around A), AO_2 and A_2O_5 (provided that the oxygens form tetrahedrons) will form glasses.

Zachariasen also addressed the formation of glasses where a network modifier, i.e. an oxide such as Na_2O that does not easily form a glass on its own, has been added. He assumed that adding the network modifier would cause the perfect network to break the A–O–A bridge and thereby form two non bridging oxygens (NBO) according to $[A-O-A + O^{2-} \rightarrow A-O^- \dots ^-O-A]$. The modifying cation would mainly occupy voids in the structure and only be loosely bound to the non-bridging oxygens. However, later studies revealed that the modifier cations occupied sites specific to the cation and that the environment of these sites complemented the environment of the non bridging oxygens. This prompted Greaves (10) to introduce the modified random network model (MRN). In this he asserted that the glass with network modifiers would be comprised of two interlaced sub-lattices; a network region where the connectivity and network structure is the same as in the unmodified glass, and a network modifier region made up of modifier atoms. Figure 2.4 shows a schematic 2d representation of the model. Channels of non bridging oxygens, bonded to the mod-

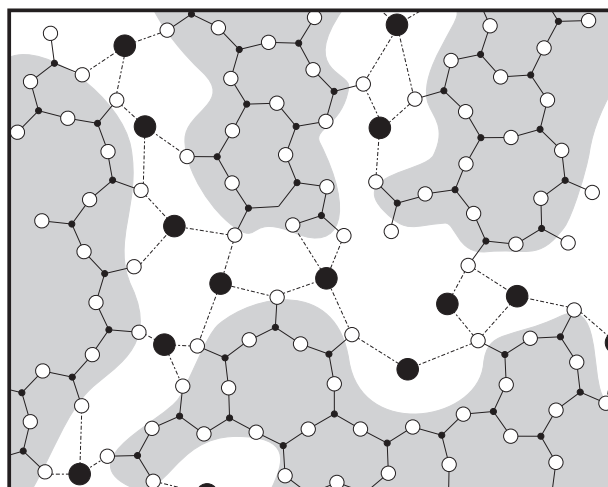


Figure 2.4: The modified random network model, with the network regions (shaded in gray) and the metal ions (black) binding to NBO:s of the network

ifier cation run through the glass. These channels are lines of easy shear and thus lower the viscosity of the glass, and if they extend throughout the glass, they can also provide pathways for ionic conduction with lower activation energy than that found in the unmodified region. The MRN model describes the network modification well for some glass formers such as silica and phosphate, but need modification in borate glasses as we shall see later. The MRN model of metal-oxide modified glass structures still stands today, supported by later studies such as Swenson *et al.* (11; 12), Cormack *et al.* (13) as well as the papers appended in this thesis.

2.2.1 Phosphate Glasses

Phosphate glasses are interesting materials due to their low T_g (as compared to silica), their ability to reach high ionic conductivity at room temperature through various additives, and their relatively high thermal expansion making them interesting for hermetic seals. A serious drawback in applications of phosphates is their hygroscopic nature where H_2O addition causes a depolymerization of the network. An oxygen bridge is then broken into two OH^- groups, similar to the depolymerization caused by M_2O modification.

Vitreous P_2O_5

The basic building block in the phosphate glass, P_2O_5 , is a tetrahedron with a central P^{5+} ion, coordinated to four O^{2-} ions, three of which are bridging oxygens, and one double bonded, non-bridging oxygen (see fig. 2.5). The P_2O_5 thus forms a 3 dimensional network where the three BO:s are shared with three other phosphate groups. (14)

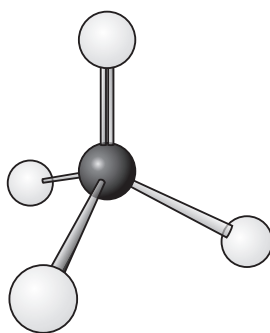


Figure 2.5: Phosphate tetrahedron, NBO at top

Oxide Modification

Addition of a network former of type M_2O with a monovalent metal ion leads to a depolymerization of the network where the added O^{2-} ion reacts with a bridging P–O–P group to create two NBO:s (15). The modified glass closely resembles the modified random network model where network regions are held together by the, compared to covalent bonds, weaker ionic NBO– M^+ –NBO bonds. This is readily seen in T_g which drops from 653 K to ca 520 K already at a 10% modification concentration in a Li_2O modified glass (i.e $R = [M]/([M]+[P])=0.1$) and reaches a minimum at ca 20% modification (14). The following increase in T_g up to $R = 0.5$ may be interpreted as an increased entanglement of PO chains.

At the metaphosphate composition, $R = 0.5$, the 3d-network has been reduced to a (theoretically) infinite 1d chain structure where all phosphates coordinate to two BO, one single-bonded NBO and one double-bonded NBO. In physical glasses however, the chains are usually restricted in length to ca 100 phosphates (with careful preparation up to 1000) terminated by a hydroxyl group. The existence of ring-shaped chains have also been proposed.

With increasing modifier content, the network further depolymerizes by shortening the length of the average chains until the $R = 1$ composition is reached, where the phosphate is reduced to individual PO_4 tetrahedra, bonded together only through the ionic $O^- - M^+ - O^-$ bonds.

2.2.2 Borate Glasses

Borate glasses are strong network formers with a relatively low glass transition temperature of $260^\circ C$ which make them suitable model systems. Highly salt doped borates reaches room temperature conductivity of $10^{-2} S/cm$ (see papers II and III). While uncommon as a major component, they are frequently mixed with other glass formers to alter their properties. In silica glasses, a borate mix provide higher mechanical, thermal and chemical stability.

Vitreous B₂O₃

B₂O₃ form a flat, triangular structure where the central B³⁺ is coordinated to three O⁻ ions which all are shared by other borons. How these triangular structures link together have been a subject of debate. One model, proposed by Krogh-Moe proposes that borate glasses largely are built up from cyclic B₃O₆ boroxol rings, experimentally supported by features of vibrational and NMR spectra. Chason *et al.* (16) have instead proposed a planar, ribbon like structure where boroxol ring may occur, but are of no significance to the model. Even today, there is no consensus of the borate structure (e.g., (17; 18; 19; 20)).

Oxide modification

Upon introduction of M₂O modifiers into the borate glass, its behavior is opposite to that of the phosphate glass. T_g actually increases with increased modification up to a modifier ratio of $R = [M]/([M] + [B]) = 0.15 - 0.20$. Likewise, the thermal expansion coefficient drops to a minimum at $R = 0.15 - 0.30$ in alkali oxide modified borate glasses, whereafter it increases rapidly (21). Both features indicate an increase in stability of the glass. The explanation is that the introduced oxygens do not break the network as in P₂O₅ systems, but instead converts the 3-coordinated borons into 4-coordinated boron tetrahedra with all four oxygens bridging. This conversion is supported by NMR (22; 23; 24), vibrational spectroscopy (25; 26; 27) and diffraction (11) investigations as well as MD simulations at various temperatures(28). At $R > 0.4$ the number of tetragonal units start to decrease while triangular units with one or two NBO increase. At the higher modifier contents, the borate structure is fairly well described by the MRN model.

2.2.3 Halide Salt Doping

A common way of increasing the ionic conductivity of network modified (M₂O)_z-A_xO_y glasses is to introduce a metal halide salt of the mobile ion, MX[†]. The resulting change in conductivity is dramatic, e.g., the room temperature dc conductivity of *x*AgI-AgPO₃ increases from ca 10⁻⁵ S/cm at *x*=0 to 10⁻² S/cm at *x* = 1.5 (29). Additionally, the introduction of the salt is commonly accompanied by a significant drop in T_g. Experimental studies have shown that the dopant ions do not participate in the network formation, and the SRO of the glass network is not significantly altered (30). This suggests that the introduced halide ions reside in the volume between the network regions and expand the channels described in the MRN model. Such a model would also explain the drop in T_g, which then is caused by the breaking of the ionic O⁻-M⁺-O⁻ bonds between different network regions due to the expansion of the channels. How the network expansion occurs is highly dependant on the type of metal ion involved, and has been a matter for controversy (see e.g. ref.

[†]Here, M is a monovalent cation, e.g., an alkali metal, Ag, Au, et c.

(31) and references therein). In papers II and III the addition of MX to $M_2O-B_2O_3$, (M=Ag, Li, Na, X=I, Cl), is discussed in greater detail.

 Ionic Conduction in Solid electrolytes

3.1 Crystalline Ion Conductors

Ionic conduction has been known for quite some time to exist in crystalline materials. The relatively simple structures of ideal crystalline ionic conductors have led to a relatively extensive knowledge of the diffusion mechanisms in these materials. The diffusion processes in most crystalline ionic crystals are dependent on the existence of crystal defects as the direct anion–cation exchange mechanism, as depicted in figure 3.1, requires a far too large activation energy to contribute substantially to the ionic mobility.

Ionic crystals can be divided into two main groups, thermally activated defect types or molten sublattice types, depending on the number of defects that participate in the conduction mechanism. In the point-defect type, the number of defects is low (10^{-5} – 10^{-3} mole per cent) and the ionic transport is mediated through thermally generated defects, mainly either Schottky pairs (32), where an anion–cation pair is missing from the lattice, or Frenkel defect pairs (33) where an ion has moved from its lattice position and resides in an interstitial position in the crystal, leaving a vacancy in the lattice, both shown in figure 3.2. The concentration of these defect types is temperature dependent and follow the same relationship;

$$c_1 c_2 = e^{-\frac{H_f - TS_f}{k_B T}}, \quad (3.1)$$

where c_1 and c_2 are the concentrations of each defect in the pair, and H_f and S_f are the enthalpy and entropy associated with the formation of a defect pair (of Schottky or Frenkel type). In a pure crystal with a low concentration of compositional impurities in relation to the number of thermal lattice defects, the concentration can be expressed as

$$c_1 = c_2 \approx e^{-\frac{H_f/2}{k_B T}}, \quad (3.2)$$

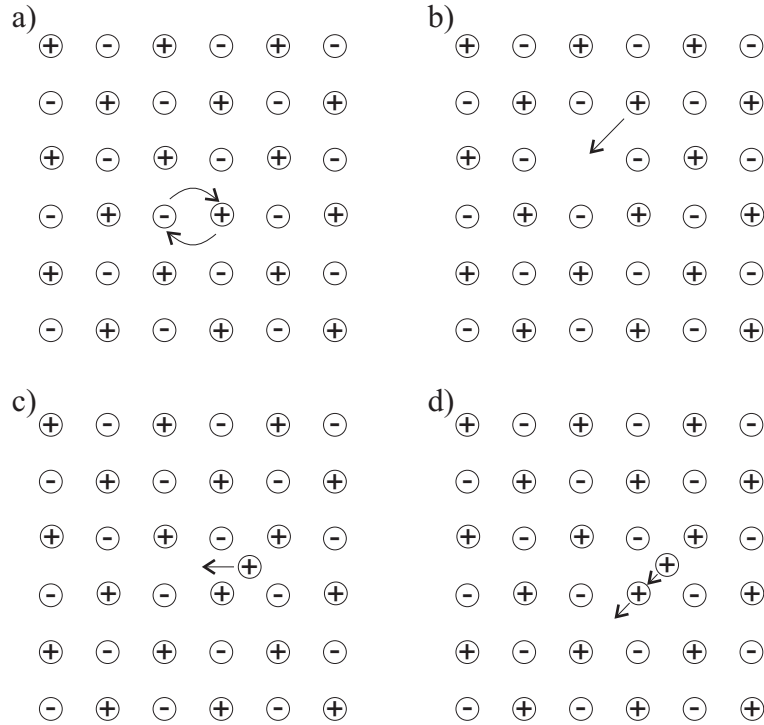


Figure 3.1: Thermally activated diffusion mechanisms in crystalline conductors; a) Direct anion-cation exchange b) Vacancy mechanism c) Interstitial mechanism and d) Interstitialcy mechanism

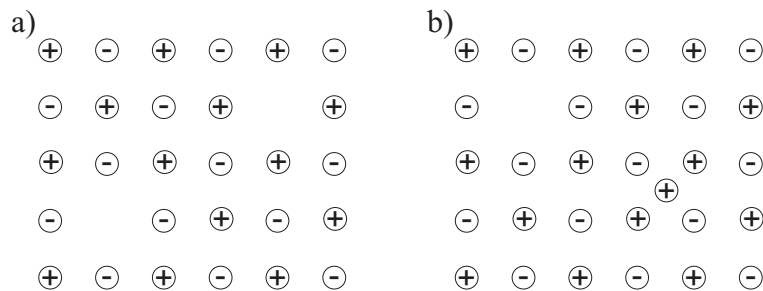


Figure 3.2: a) Schottky defect where an anion-cation pair is missing from the crystal and b) Frenkel defect pairs of a (here) cation who migrated from its ideal position, leaving a defect behind.

Since the number of charge carriers is directly related to the total conductivity, it will also follow an Arrhenius behavior in this case.

Figure 3.1(b–d) displays three commonly cited, defect mediated diffusion mechanisms in solids with a low defect concentration. In the vacancy mechanism (figure 3.1b) a nearby ion jumps into a Schottky vacancy, leaving a new vacancy in its wake, a process that equally well can be described as the diffusion of a vacancy defect through the lattice. In the interstitial mechanism (fig. 3.1c) the ion moves between interstitial sites, whereas in the interstitialcy mechanism (fig. 3.1d) an ion moves from an interstitial site to an occupied lattice site, thereby pushing the ion residing at that position into another interstitial site. Apart from these three, there are also suggestions for mechanisms involving several ions at interstitial sites.

In the molten sublattice type of FIC, with a high defect concentration, the defects are not generated by thermally induced disorder. In these materials, there is a large number of possible sites for mobile ions and they can diffuse freely in this sublattice of vacancies. A prime example of such materials is the high-temperature α -phase of AgI. Here, the iodine ions form a regular body-centered cubic lattice with a total of six energetically equal Ag sites per Ag ion. This abundance of vacant sites form the molten sublattice and due to the much smaller size of Ag vs I ions, Ag ions are free to jump to any one of the four nearby sites with a low probability that the target site is occupied*. The activation energy is here related to the energy barriers in the potential landscape and not the creation of vacancies and charge carriers.

While the mechanisms of conductivity have been known for quite some time (Frenkel and Schottky presented their work in 1926 and 1935), the interest in crystalline ionic conductors was quite low since most known crystals showed a low conductivity. This changed in the mid 1960th with the discovery of several fast silver ion conductors (35). Among them RbAg_4I_5 (36; 37) with a room temperature conductivity exceeding 0.1 Scm^{-1} , to this day the fastest known solid RT conductor (see fig. 3.3). These materials all exhibit a molten sublattice mechanism for the Ag conductivity. These new materials were hoped to facilitate new types of batteries and fuel cells, a rapid expanding field during the 1970th oil crisis, but they have yet to fulfill these promises. Primarily this is due to the difficulty of producing single crystals in the desired shape or large enough sizes for many applications. Problems that glassy FIC (to some extent) do not have.

3.2 Conduction Models in Glasses

Glassy ion conductors are of interest due to the desirable properties they have over crystalline materials, many of which already are covered in chapter 2. These include the possibility to fine tune their mechanical, thermal and conductive properties by introducing different types of additives, as well as the ease of producing thin films in desired shapes on substrates by sputtering or vapor techniques etc. The fastest

*3-dimensional visualizations of the Ag diffusion pathways are shown in figure 5.3 (calculated by the BV method) and in ref. (34) (first-principles MD)

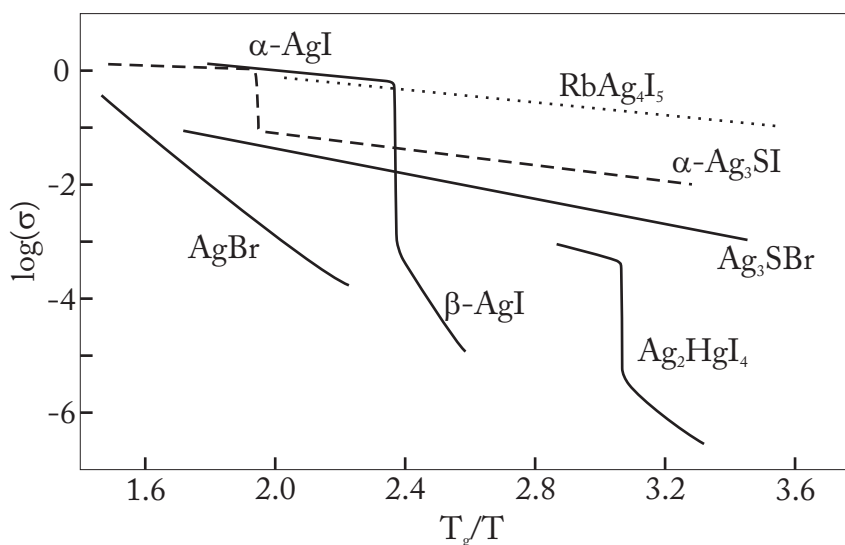


Figure 3.3: DC conductivity for a number of crystalline FIC materials. The discontinuities are due to phase transitions, e.g., the α - β transition of AgI

conducting glasses display room temperature dc-conductivities of up to 10^{-2} S/cm, which make them interesting for applications as solid electrolyte in, e.g., micro-scale batteries. However, unlike the crystalline ion conductors, the conduction mechanism in glasses still lack a universally applicable theory. Several models have been proposed and I will here give a short overview of a few of them.

The earliest models were influenced by the structural models available at the time. Starting from the micro crystalline or crystallite structural models, it would of course be natural to use the models for conduction in crystalline materials, referring to the corresponding crystalline mechanics, but as these structural models fell out of flavor, so did the corresponding conduction models. Almost the opposite is suggested in the cluster bypass model (38; 39) which asserts that small liquid regions remain in the glass even below T_g , and fast ion conductivity is related to liquid-like diffusion through liquid channels in the glass. Indeed somewhat bold to propose that liquid-like relaxations may take place at these temperatures. The cluster model and the diffusion pathway models both address the highly conducting AgI doped glasses by assuming that regions of iodines are formed providing Ag with mainly iodine coordinated, low E_a , conduction pathways. In papers II and III, however, we find a preference for mixed coordination of the Ag ions.

Other models of conductivity deserve a more in-depth discussion. The weak and strong electrolyte models are of a great conceptual value in explaining the origin of the activation energy, E_a , and the dynamic models (dynamic structure model, jump relaxation model and the unified site relaxation model) have had some success in explaining the origin of the mixed mobile ion effect, discussed in section 3.3. The bond-valence method, which we have used ourselves, will be discussed later in section 5.2

3.2.1 The Anderson-Stuart Model

The total conductivity in an electrolyte may be expressed as

$$\sigma = Ne\zeta\mu, \quad (3.3)$$

where N is the density of mobile ions, $e\zeta$ is the charge of each ion and μ is the mobility. There is thus two different contributions that may lead to the temperature dependent behavior of ionic conductivity; either there is an increase in the number of mobile ions with increasing temperature or there is an increase in the mobility of each ion.

The Anderson-Stuart (A-S) model (40) (or strong electrolyte model as it is also called) assumes that the mobile ion concentration is roughly constant due to a full dissociation between the mobile ions and the network (or salt in the case of a doped glass). The activation energy is here identified as a combination of a strain energy and a Coulomb attraction energy that an ion must overcome to jump from one site to the next.

Thus, for an ion to move from a site at anion A to anion B, it must first overcome the energy of Coulomb attraction from the anion at the A-site, E_c . Furthermore, a strain energy E_s is associated with the opening of a doorway, i.e. moving the two BO:s in the center of figure 3.4 aside, to allow the cation to pass through. The total activation energy for the jump is then the combination of these two energies.

3.2.2 Weak Electrolyte Model

The weak electrolyte model instead assumes that there is a low dissociation of mobile ions in the glass. If the number of mobile ions is low, then the mobility is independent of N and the conductivity is directly proportional to the number of mobile ions.

If we view the conducting glass as a solid solution in which the network, or dopant salt, behaves as a weakly dissociated electrolyte, then it should follow the dissociation equilibrium:



implying that the concentration of mobile ions, $[M^+]$ is given by

$$[M^+] = \sqrt{Ka_{M_2O}}, \quad (3.5)$$

where K is the dissociation constant and a_{M_2O} is the thermodynamic activity of M_2O . Since only the dissociated M^+ ions are mobile, the conductivity of a glass should correlate to the activity, which it has been shown to do for different silica glasses(41). The activation energy in this model thus has two contributions; an activation energy of mobility (similar to that of the A-S model) and the energy required to dissociate from the oxide (or salt).

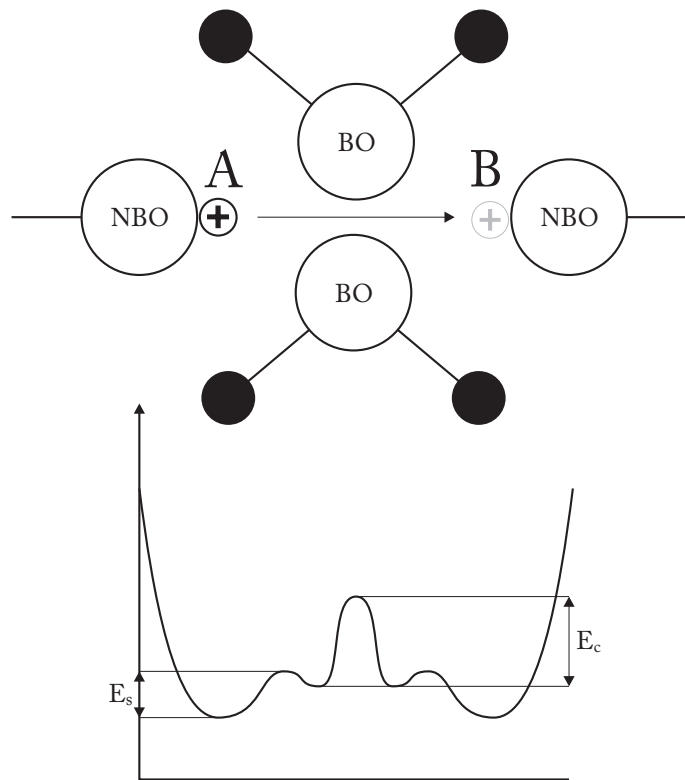


Figure 3.4: Schematic of the Anderson-Stuart model.

3.2.3 Dynamic Models

Dynamic Structure Model

The key features of the dynamic structure model (42; 43; 44) are:

1. The glass network is not completely frozen in, until far below T_g
2. The mobile ions create their own environment and thus shape the glass structure
3. The ionic conduction is a hopping process

Its idea is that structural relaxations are not only possible, but a major part in the explanation of the observed conduction pathways in glasses. In a glass with mobile ions of type A, these ions will predominately occupy \bar{A} sites which are energetically favorable sites for A ions in terms of coordination numbers and bond length. There are other sites in the lattice, called \bar{C} sites which are less energetically favorable for A occupation, but the energy mismatch is not large enough to forbid A occupation. Should an A ion hop from its site to a \bar{C} site, the energy difference will make a correlated backward jump likely, but if the ion resides in the site long enough for the coordinating anions to relax, it can adapt the \bar{C} site into an \bar{A} site. Meanwhile, the \bar{A} site left behind is now in an energetically unfavorable state and will thus relax into a low energy \bar{C} site.

The nature of the model makes it highly suitable for Monte Carlo simulations, where a simple square grid of \bar{C} sites are populated by mobile ions. By assigning a relaxation time for the $\bar{C} \rightarrow \bar{A}$ relaxation, and likewise the $\bar{A} \rightarrow \bar{C}$ relaxation and let the ions hop randomly between the sites (with an energy dependent probability) a network of path will form as a region of \bar{A} sites are more frequently occupied by A ions and hence less likely to relax to \bar{C} sites. Furthermore, the model offers explanation for the mechanism of a cooperative conduction process and a threshold in the conductivity since a small number of mobile ions cannot uphold a continuous pathway network.

The model was also early adopted for the mixed alkali effect by introduction of B ions and the corresponding \bar{B} sites. Monte carlo simulations managed to reproduce both diffusion coefficients of both ionic types but also the ac conductivity.

However, despite its numerical success, the model can be called into question on its bold statement that the ionic motion to any degree couples to the relaxation of the glass matrix below the glass transition temperature, a question raised even by one of its original authors (45). Angell (46) has pointed out that there is a decoupling between ionic and structural relaxations at temperatures below T_g . The timescale of the structural relaxation time at T_g , whereas the ionic relaxation time may be as fast as 10^{-9} s. While the DSM may be applicable to glasses above T_g , its validity below it should not be taken for granted.

Jump Relaxation Model

The jump relaxation model (JRM) by Funke (47; 48) approaches the hopping process in glasses with a strain energy associated with the jump to a new site, akin to the DSM model. A fundamental difference is the physical origin of the strain energy at the new site, and the following relaxation. In JRM, the energy mismatch is assumed to originate from the Coulomb field of the other mobile ions in the glass. This is a fully reasonable hypothesis considering that in an equilibrated material with mobile ions, the ions will be distributed as to minimize the potential energy of the system. For Coulomb interactions, this will be the distribution that minimizes the fluctuations in the electric field. If one of the ions jumps to a new site, a local disturbance in the force is induced. Assuming a much shorter relaxation time for the ions than the glass matrix, the distortion of the field can be normalized, either by a backward jump of the ion, or a movement of the surrounding ions.

JRM was developed with the frequency-dependent conductivity in mind and do provide a model that fit to experimental data while providing a microscopic explanation for the behaviour.

3.3 Mixed Mobile Ion Effect

One of the puzzling problems in trying to construct a universal model for ion conduction is the *Mixed Mobile Ion Effect* (49; 50) (MMIE, also known as the Mixed Alkali Effect). While there is no direct correlation between the composition and

properties of oxide glasses, in many cases a given property will change in an approximately linear fashion as composition is varied between two end compositions, A and B . To a first approximation the property G of an intermediate composition can usually be taken to be

$$G = c_A G(A) + c_B G(B), \quad (3.6)$$

where c_A and c_B are the relative concentrations of A and B respectively. This is however far from true in some mixed systems.

A good example of this is the strong non-linearity in ionic conductivity as Li_2O is exchanged for Rb_2O in the metaphosphate glass system $(\text{Li}_2\text{O})_{1-x} - (\text{Rb}_2\text{O})_x - \text{PO}_3$. At room temperature, σ_{dc} drops a good 8 decades below that expected from equation 3.6 at the intermediate $x = 0.5$ composition. In general, properties related to the mobility of the metal ions in metal-oxide modified glasses, such as conductivity, dielectric loss, T_g^\dagger , thermal conductivity and viscosity (6; 52; 50), tend to show a non-linear behavior. Meanwhile, other properties such as density, sound velocity and optical properties vary slowly and approximately according to equation 3.6 (53; 50). Although the discussion here will be restricted to MMIE in glassy systems, it has been observed also in crystalline materials (e.g., (54; 55)). While a complete model of the MMIE by necessity must be able to explain all of its aspects, we will here focus our attention to the MMIE on dc-conductivity.

Several models have been proposed for the MMIE, but so far none have made claim to explain all of the properties of MMIE. Early structural models speak, e.g., of phase separations between alkali rich and alkali poor glass regions, better chances for differently sized ions to find low energy sites etc. More bond and coordination centered theories instead point to, e.g., differences in field strengths or mass differences of ions (see review: (49)). These models have however not been able to reproduce experimental data to any degree, or have had too many free parameters to have any physical meaning. Any real advancement in the understanding of the MMIE came first with the availability to computers and simulations on larger scale.

Today, a consensus have more or less been reached that there are preferential diffusion path for different kinds of ions in a mixed glass. The more different the two ions are in size and polarizability, the more different will their preferred coordination environments, or sites, be. Molecular orbital computations have shown an energy penalty for an ion to jump into an site adopted for another ion type (56). The idea of an energy penalty for an ion to occupy an unlike site is also an integral part of the dynamic structure model. The source of this penalty is however an open question.

The dynamic structure model has been applied to the MMIE problem with some success. as described above. It has managed to reproduce the diffusion cross over of the two mobile ions, and the conductivity drop, but as described above, its fundamental assumptions of a highly adaptive glass matrix at the timescale of ionic movement may be overstated in glasses below T_g .

[†]It should be noted that in, at least, mixed alkali-phosphate systems, T_g experiences a minimum at the mixed composition. A non-intuitive behavior considering that this is where the ionic mobility is the lowest. (51), Paper IV and refs. therein

MD simulations of mixed alkali silicates at 700 K by Habasaki and coworkers (57; 58; 59) do not find site conversions to the extent required by the DSM. Instead, the existence of local structures, characteristic to each ion and a separation of pathways with a stability of several hundreds of picoseconds are found, in line of preferential diffusion pathways. The MMIE is proposed to be caused by a mutual interception of the jump paths. These findings are in agreement with bond valence calculations of $\text{Li}_x\text{Rb}_{1-x}\text{PO}_3$ in which the ion types are found to block of each others pathways. Additionally, the efficiency of the blocking is enhanced by the low dimensionality of the pathways(60; 61).

As briefly mentioned above, the difference in mass was once thought to be one of the factors that contributed to the MMIE. An investigation of a mixed $^6\text{Li}/^7\text{Li}$ borate glass did show a pronounced effect(62) but the result was later refuted by other groups (63; 54; 64). However, this may not be the end of the story. In paper V, an investigation of the MMIE in the mixed $\text{Ag}_x\text{Na}_{1-x}\text{PO}_3$ system, which exhibit a very low MMIE, we propose that the mass difference may play a role in this system. The two ions share a large part of their pathways, and can thus participate in an inter-specie cooperative hopping process (ISCH). The Ag and Na ions are similar in preferred coordination environment, but differ in weight by a factor of four. The mass difference is dramatically larger than in the $^6\text{Li}/^7\text{Li}$ system and may thus play a part in the MMIE. Indirect support is given by a 2d simulation of Brownian motion (65) with an ion mass ratio of 1/3. While the simulation is a simple microscopic flow model, it does reproduce a compositional dependence of the diffusion in the system.

While the MMIE still is not understood fully, a better understanding of it have been gained in the past 15 years. The existence of distinct pathways for different ions is mostly agreed upon, and so is the idea of an energy penalty for a jump to an unlike site. The question that is under debate is whether the suitable sites are frozen in at the glass transition, or if they are created by the mobile ions themselves.

CHAPTER 4

Experimental Probes

None of the structural knowledge of glasses we have today would be possible without the wealth of experimental data we have at our disposal. The strength lies not in any specific experimental technique, but in the varied and complementary structural information they can provide. Diffraction techniques (sect. 4.4) are useful for information on the average atomic distribution on length scales of typically 1-30 Å (although longer length scales are possible). Atom specific techniques such as XAS (X-ray absorption spectroscopy) and NMR (nuclear magnetic resonance) are the perfect complement as these provide detailed information on coordination environments of specific atoms. Vibrational spectroscopy gives information on the dynamics of specific groups (e.g., a P–O bond vibration) and changes in these vibrations when e.g. composition or temperature is varied. Even macroscopic properties, such as density, T_g et c., can provide us with clues on what is happening on an atomic scale with a change in sample composition.

Here, we will discuss each of these experimental groups separately, focusing on the diffractive techniques, and thermal analysis used in the attached papers.

4.1 Macroscopic Scale Probes

At the macroscopic scale we can measure properties such as mechanical strength, density, thermal expansion and color. While these may not initially seem useful for structural determinations, their dependence on microscopic properties (bond strength and topography, impurities et c.) makes it possible to relate these properties (albeit indirectly) to the microscopic structure. Of particular interest is to measure differences when a small change of the sample is made, such as compositional, temperature or means of production.

Measurements of thermal properties belongs to this group as well and can pro-

vide valuable knowledge about changes in bonding due to compositional changes (as discussed in the section 2.2.2) The most commonly used technique for thermal analysis is today Differential scanning calorimetry.

4.1.1 Differential Scanning Calorimetry

For investigations of the thermal properties of glasses, differential scanning calorimetry (DSC) is often used. In principle, DSC is rather simple. By heating a sample at a constant rate of change in temperature and measuring the heat (in W) needed to do so, any process that involve a change in thermal properties can be detected. A step-wise change in the heat needed indicates a change in the heat capacity, C_p , which is a measure of the internal degrees of freedom in the system. If the heat instead is changed only over a short temperature interval, we either have an endothermal (increased heat) or an exothermal (decreased heat) process in the sample.

Practically, the measurement of a sample is performed in a sample holder, (pan), and thus the required heat is usually expressed as the difference in heat flow to the sample and pan as compared to a reference (usually an empty pan). Current instrumentation, such as the Q1000 DSC from TA Instruments we have used, are not only capable of heating, but also cooling samples and perform multiple heating/cooling cycles to investigate any hysteresis behavior of the sample (due to chemical reactions, crystallization of glasses etc). In addition new DSC techniques such as temperature modulated DSC can improve the resolution of the thermal processes.

Figure 4.1 shows a schematic DSC curve for a glass-containing sample during a heating cycle. As pointed out in the earlier discussion on the glass transition (section 2.1) it is characterized by a rapid change of C_p and is seen as a step in the curve. At T_c , a crystallization, which is an exothermal process, gives a peak in the curve while the endothermal melting at T_m gives a corresponding dip of the curve.

Quantitative information can be extracted from these curves. E.g., an integration over a melt peak yields the total energy required for the phase transition i.e. the latent heat associated with the transition.

4.2 Vibrational Spectroscopy

Molecular vibrations present in a sample can give valuable information of its structure. Many vibrational modes yield strong signals and are relatively sensitive to the exact structure and can generally be identified. One such mode is the -O-H vibration which for our purposes can be used to detect, e.g., the extent of depolymerization by water of a phosphate glass, and thereby gain knowledge of its integrity. Two vibrational spectroscopy techniques are commonly used; Infrared (IR) and Raman.

Although infrared and Raman spectroscopy are two different techniques concerning the way radiation interacts with the sample, they are usually mentioned together since both of them are used to study the vibrational spectrum, and due to their different physical origin, they are complementary to each other.

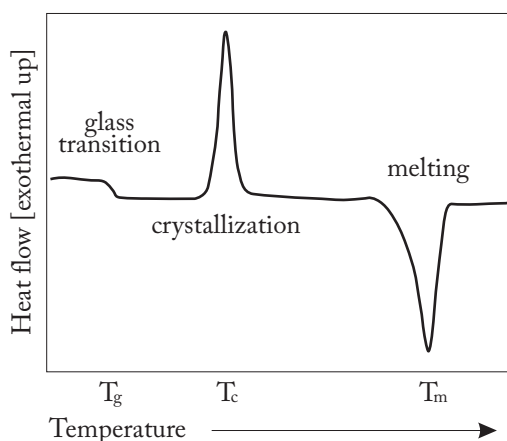


Figure 4.1: Schematic DSC curve showing typical responses to; glass transition, crystallization and melting, during a heating cycle.

In infrared spectroscopy, a broad spectrum of infrared light passes through a sample and an absorption spectrum is obtained by comparing the signal after the sample to a reference signal. In the infrared region, light is absorbed by the molecules by a change of their vibrational states. However, not all state transitions can be induced by an absorption. For a vibrational transition to be IR-allowed, the change in vibrational state must also give a change in the dipole moment of the molecule. Example of allowed IR transitions are the asymmetric stretching modes in a coordination tetrahedra, or the O-H vibration in a hydroxyl group.

Raman spectroscopy, on the other hand, is a process where the molecules scatter incident monochromatic light, usually in the visible region of the spectrum. In Rayleigh scattering, the molecule is excited by the incident light and immediately relaxes down to its original state. If, however, the molecule does not relax to the state it came from, we have inelastic Stokes or anti-Stokes scattering, where the energy difference corresponds to a Raman allowed transition with a change in the polarizability of the molecule. This gives that Raman shows strong peaks for non-polar functional groups and thereby complements IR data.

Raman and IR usually share common absorption bands, but complementing measurements with both techniques give more information on the vibrations in the material. A fundamental difference is however, that IR uses transmission and the sample must therefore be more or less transparent, whereas Raman can be done by studying the scattering from a surface.

Both Raman and IR can be used to study the vibrations in amorphous materials. Structural information, such as the location of a metal ion in a modified glass can be seen by, e.g., a shift in a vibration (compared to the undoped glass) of a group, coordinated to the ion.

4.3 Atom Specific Probes

Apart from the neutron and X-ray diffraction methods, there are a wide range of different structural probes that can give important pieces of the puzzle. Where neutron and X-ray diffraction typically fall short is on the short range order of amorphous materials exhibiting several different interatomic correlations on a similar length scale. Element specific probes such as XAS and NMR can give wealth of information on coordination numbers and bond length to complement the diffraction methods above.

XAS (X-ray absorption spectroscopy) and the closely related EXAFS and NEXAFS ((near-edge) extended X-ray fine structure) all probe the anomalous scattering near an X-ray absorption edge of the element of interest, where the absorption is slightly different depending on the environment of the atom. In pre-edge XAS, the studied electrons are excited at slightly lower energies than the absorption edge of the isolated atom due to changes in the electron structure caused by its neighbors. The technique is predominately useful for transition metals where ligands affect the energy splitting of d- and f-orbital electrons. Post edge x-ray absorption (EXAFS, NEXAFS) is caused by a back scattering of photo-electrons and results in a oscillating behavior at energies above the absorption edge. These techniques provide information on the closest environment in terms of number of neighbors and distances to atoms in the first and second coordination shell.

NMR (nuclear magnetic resonance) utilizes the magnetic spin of the atomic nucleus. A nucleus of, e.g., ^{13}C has two spin states, up and down, which normally are degenerate. Under a magnetic field however, the two states will split with an energy ΔE thereby causing the lower energy state to have a higher population. An electromagnetic wave with an energy ΔE can thus excite a nucleus in the low energy state and the population relaxation can be measured. The energy shift is dampened by the magnetic shielding the electrons around the nucleus provide. If the probed atom is in a solid, the electron cloud, and hence the shielding, is distorted by any coordinating atoms whereby the resonance frequency shifts slightly (so called chemical shift). Information on structure can thus be obtained by assigning absorption peaks to different kinds and number of ligands.

4.4 Diffraction Techniques

X-ray and neutron diffraction have become important standard tools in the investigation of the structure of amorphous and complex materials. These let us investigate the atomic distribution within glasses and together with computational structure modeling, e.g., reverse Monte Carlo (see sect. 5.1.3) we can build detailed structural glass models. While both diffraction techniques essentially work on the same principles the two are often complementary to each other as the interaction between neutrons and the sample is slightly different from that of x-rays.

X-rays are scattered against the electrons surrounding the atoms and thus the form factor is roughly proportional to the atomic number. This means that corre-

lations between heavy elements, such as silver and iodine, dominate the scattered intensity. Neutrons are however scattered against the atomic nucleus and the scattering length depends strongly on the exact energy levels of the core. The scattering lengths thus vary in an erratic way along not only the elements but also with the isotopes. In the case of AgI doped borate glasses, the neutron diffraction experiment shows mainly correlations involving borons and oxygens, whereas the natural isotopes of both silver and iodine contribute very little to the total scattering. The X-ray diffraction data are however dominated by the heavier atoms.

A third diffraction technique, which will not be covered in any detail, is electron diffraction. Electrons are easily absorbed by most substances and electron diffraction in a reflection geometry can thus provide information from the very top layers of the sample. Additionally, an electron beam can be focused to a much smaller spot than either X-rays or neutrons and is thus a highly local probe of the structure. It does however come with some strong limitations. Any experiment must be conducted in vacuum to minimize unwanted interactions with the environment, a requirement that is unsuitable for, e.g., volatile liquids. Furthermore, non-conducting materials will quickly be locally charged, leading to an interaction of incident electrons not only with the atoms themselves, but also by the Coulomb-field from the local electrostatic charge.

For a more in depth review of diffraction techniques, see e.g. (6; 66; 67).

4.4.1 Neutron Diffraction

Neutrons are uncharged particles and their interaction with an atom is largely an interaction with the nucleus. Neutrons do however carry a magnetic spin, something that is sometimes used to probe the magnetic structure in a sample, but this will not be covered here.

A neutron, incident on the sample is characterized by its momentum, \mathbf{k}_0 . If an interaction between the sample and the neutron occurs (as displayed in figure 4.2), it can be described in terms of its momentum, \mathbf{Q} , and energy transfer, $\hbar\omega$, which are defined by

$$\mathbf{Q} = \mathbf{k}_0 - \mathbf{k}_1 \quad (4.1a)$$

$$\hbar\omega = \frac{\hbar^2}{2m} (\mathbf{k}_0^2 - \mathbf{k}_1^2) = E_0 - E_1. \quad (4.1b)$$

If a sample of N atoms placed in a neutron beam of density current j_0 has j events per second, then the *scattering cross-section* of each atom (assuming single component sample), σ is

$$\sigma = \frac{j}{j_0 N}. \quad (4.2)$$

The dimension of σ is area and represent the effective area, perpendicular to the neutron beam, that a neutron must hit in order for an interaction to happen. This can either be in the form of an absorption or a scattering event, and we can write the total cross section as a sum of the two: $\sigma = \sigma_s + \sigma_{abs}$

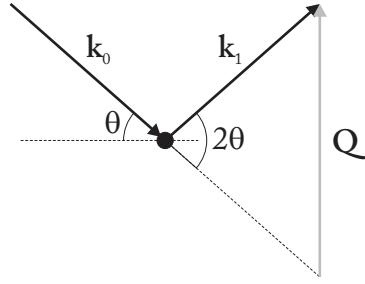


Figure 4.2: Elastic scattering process where \mathbf{k}_0 is the incident particle, \mathbf{k}_1 is the scattered and \mathbf{Q} is the momentum transfer

The scattering cross-section is in turn related to the quantity b , called the *scattering length*.

$$\sigma_s = 4\pi\langle b^2 \rangle. \quad (4.3)$$

The scattering length is dependent on, not only the element, but also the isotope since its interaction with the nucleus is related to the occupation of its energy levels. The variation does, however, not follow any clear trend and b varies erratically with the isotopes, even taking on negative numbers. This is an important feature of neutron diffraction. If a neutron diffraction experiment is conducted on two samples of a pure borate glass, one containing only ^{10}B and the other only ^{11}B , equation 4.2 states that when we change isotope, and hence the scattering length, there will be a difference in $S(Q)$. The two samples will be nearly identical in their structure, since the bonds are determined by their chemical properties so any measured difference in $S(Q)$ is related to the boron correlations alone.

By defining the two averages $\langle b^2 \rangle = 1/N(\sum_i b_i^2)$ and $\langle b \rangle^2 = 1/N^2(\sum_i b_i)^2$ where the sums are over all isotopes of a particular element, we may rewrite σ_s , which can be separated into a coherent and an incoherent part as

$$\sigma_s = 4\pi\langle b \rangle^2 + 4\pi(\langle b^2 \rangle - \langle b \rangle^2) \quad (4.4)$$

The rightmost term in this expression is the so called incoherent scattering cross-section σ_{inc} , and contains correlations between a single nucleus at the time $t = 0$ and some later time. Note that the incoherent scattering is zero if only one isotope is present in the sample. The left term $\sigma_{coh} = 4\pi\langle b \rangle^2$ is the coherent scattering cross section which contains correlation between an atom at $t = 0$ and itself at a later time, but also correlations to all other atoms at $t = 0$ and later.

In a neutron scattering experiment, we measure the double differential scattering cross-section which is the probability that an incident neutron will scatter into the solid unit element $d\Omega$ in the solid angle Ω while having an energy in the range $[\hbar\omega, \hbar\omega + \hbar d\omega]$ and can be written as

$$\frac{d^2\sigma}{d\Omega dE} = \frac{1}{\hbar} \left(\frac{d^2\sigma_{coh}}{d\Omega dE} + \frac{d^2\sigma_{inc}}{d\Omega dE} \right) \quad (4.5)$$

where

$$\begin{aligned}
\frac{d^2\sigma_{coh}}{d\Omega dE} &= \frac{k_1}{2\pi k_0} \langle b \rangle^2 \int_{-\infty}^{\infty} e^{-i\omega t} \sum_{m,n=1}^N \langle e^{-i\mathbf{Q}\mathbf{r}_n(0)} e^{i\mathbf{Q}\mathbf{r}_m(0)} \rangle_T dt \\
&= \frac{k_1}{2\pi k_0} \langle b \rangle^2 \int_{-\infty}^{\infty} e^{-i\omega t} S_{coh}(\mathbf{Q}, t) dt \\
&= \frac{k_1}{2\pi k_0} \langle b \rangle^2 S_{coh}(\mathbf{Q}, \omega)
\end{aligned} \tag{4.6}$$

The corresponding expansion for the incoherent part is calculated similarly but with the substitution $\langle b^2 \rangle \rightarrow \langle b^2 \rangle - \langle b \rangle^2$

The inelastic incoherent scattering contains dynamical information about the material, but in the static approximation, an integration over all frequencies it will only add a constant background.

The coherent structure factor is related to the real-space van Hove correlation function $G(\mathbf{r}, t)$ through the double transform

$$S_{coh}(\mathbf{Q}, \omega) = \frac{1}{2\pi\hbar} \int G(\mathbf{r}, t) e^{i(\mathbf{Q}\mathbf{r} - \omega t)} d\mathbf{r} dt \tag{4.7}$$

where $G(\mathbf{r}, t)$ describes the correlation of particles at $(\mathbf{r}, t = 0)$ to the particles at $(\mathbf{r}', t = t')$. It can be written as

$$G(\mathbf{r}, t) = \frac{1}{N} \sum_{ij} \int \langle \delta(\mathbf{r}' - \mathbf{R}_i(0)) \delta(\mathbf{r}' + \mathbf{R}_j(0)) \rangle d\mathbf{r}' \tag{4.8}$$

where \mathbf{R}_j is the position of particle j and the average is taken over temperature. The van Hove correlation function can be divided in to parts; a self correlation, which is the correlation of a single particles time evolution and the pair correlation (or distinct correlation).

An integration over all frequencies in equation 4.7 yields the static $G(\mathbf{r}, t = 0)$, i.e. the average particle correlation and is related to the static structure factor by

$$S(Q) = 1 + \frac{4\pi\rho_0}{Q} \int_{-1}^1 (G(r, 0) - 1) \sin(Qr) r(d)r. \tag{4.9}$$

4.4.2 X-ray Diffraction

In X-ray diffraction, the X-rays interact with the electron cloud surrounding the atoms in the sample. Since the electrons are distributed over a volume whose length scale is similar to that of the incoming radiation, this case can not be considered scattering against a point particle as for neutrons. Scattering contributions from different parts of the electron cloud will interfere with each other and the scattering strength, or form factor, f , as it is called in X-ray scattering, shows a strong dependence on the scattering vector \mathbf{k} (\mathbf{Q} in figure 4.2), with a monotone decrease with increasing $|\mathbf{k}|$. The scattering strength of atoms increases with increasing number of electrons

and thus for a multi component system, the scattered intensity is weighted towards correlations involving heavy atoms.

Furthermore, for a multi component system the transformation from reciprocal to real space correlation functions (the inverse transform of equation ??) is not possible to calculate exactly from the X-ray structure factor $F(k)$ due to the strong angular dependency of the form factor and its variation among atoms. Since the form factor decreases with increasing values of k , it may be difficult to obtain high k -range data from X-ray diffraction due to a low signal-to-noise ratio at high scattering angles.

Structural Modeling and the Bond Valence Method

5.1 Modeling Amorphous Materials

Computers have allowed us far more refined ways of creating structural and dynamic models of complex materials than what could have been achieved otherwise. Molecular dynamics provide not only structures but also the dynamics of the system, and allows a detailed study of the movement of individual atoms. Monte Carlo methods creates static structural models but at far less computational costs. These methods are commonly used for large structural models (containing thousands of atoms) while other methods, such as molecular orbital or ab initio typically focuses on providing detailed information on processes through quantum mechanical computations. There is always a constant development and sometimes merger of these techniques. E.g., in later years, ab-initio MD have risen due to the ever increasing computational power available in research.

Here, we will look closer at three of these modeling techniques.

5.1.1 Molecular Dynamics

The perhaps most natural method of computer simulations of a material is the Molecular Dynamics simulation (MD) (Alder, '57; Alder, '59; Alder, '60). Since the systems we are interested in simulating here are composed of atoms which have relatively large masses and low velocities, their motion can be treated classically. The time evolution can then be calculated by Newtonian physics where the motion of each atom is governed by

$$m_i \ddot{\mathbf{r}}_i = - \frac{\partial U_{pot}}{\partial \mathbf{r}_i} = \mathbf{f}_i \quad (5.1)$$

, where m_i is the mass of particle i , \mathbf{r}_i its position, ∂U_{pot} is the potential energy and \mathbf{f}_i is the force acting on the particle. In the most general case the potential landscape

∂U_{pot} in which the atom moves depends on the location of all $N - 1$ other atoms in the system (neglecting possible force fields outside the system). To determine the time evolution of the system, we must solve the system of the N coupled differential equation in eq. 5.1. Molecular dynamics is simply put a numerical integration of this equation system. Commonly the Verlet algorithm (Verlet, '67) is used in implementations due to its stability.

In order to simulate the full movement of atoms, each time step in the integration must be significantly shorter than the period of any atomic (vibrational) movement, and thus for most systems the time steps are of the order of 10^{-15} s. This short time step makes simulations of any larger system or during a longer simulation times (> 1 ns) computationally expensive.

As with any computer simulation method, we must choose a start configuration of the material we are simulating, and make sure that this choice will not affect the final result. In crystalline materials the atoms may be placed according to the ideal crystalline structure and given a random Maxwell distribution of velocities according to a target temperature, but for glasses this is not possible as we do not know the structure beforehand. Instead, the glass structure model is built in the same way as real glasses are, i.e. by starting with a melt at an elevated temperature (a few 10^3 K), where the atoms are allowed to mix during an equilibration period, and then quenching the melt into a glass. This change of temperature during the quench is of the order of 10^{12} K/s, a far more rapid quenching than what normally is achievable (10^9 K/s during sputtering), and thus an MD glass model may be expected to have a higher residual entropy than a real glass.

Once a configuration that does not explicitly depend on the start configuration has been reached, the model and its time evolution may be used to obtain information on the system. Early applications involved computing various thermodynamical quantities by averaging the observable quantities over the system trajectory and apply the ergodicity hypothesis, which states that the time average of a quantity of a system is equivalent to its average over a statistical ensemble. However, since the MD simulation contains detailed information on the movements of each atom, much more data may be extracted. Relevant for this work is the studies of diffusion and conduction processes in glassy materials, where MD can contribute with information not available elsewhere. For instance, Jund *et al.* (68) have studied the paths taken by the mobile ions of a glass and could thereby create pathways for ionic diffusion and the details of ionic jump processes. More detailed studies of the equilibrium sites between which the ions jump have been performed by Vogel (69) and Lammert (70) among others.

The MD method is however not without problems. The simulated system is, as is the case for most computer simulations, of a finite size (typically a few thousand atoms, although models with up to 10^6 atoms have been simulated (71)), and thus boundary effects may be of importance for the results. For simulations of bulk systems, this is usually solved by implementing periodic boundary conditions, i.e. the simulation box is surrounded by 26 identical boxes. This reduces the problem, but effects of the limited size may still arise and must be taken into consideration.

Numerical inaccuracies may also cause some problems in the calculations and, if not accounted for, may cause a drift in temperature even for adiabatic systems.

However, the largest problem to obtain good MD models lies in the choice of realistic interaction potentials. Simple liquids can be simulated with reasonable results by hard sphere, or two-particle Leonard–Jones potentials (72), but for complex solids like ion conducting glasses these do not suffice. Commonly, potentials used for glass simulations are extracted as two-particle potentials from binary crystals containing the atoms of interest, and asserted to be the same in the glassy structure (13). There are also models where the interaction potential is computed by quantum mechanical (QM) methods, such as ab-initio MD (73), where density functional theory (DFT) is used for the electronic degrees of freedom. QM methods are however several orders of magnitude slower than classical approximations, and thus cannot be used for large systems under long simulation times.

5.1.2 Metropolis Monte Carlo

A reoccurring problem in condensed matter physics is to compute various thermodynamical quantities. To compute the equilibrium value of an observable \mathcal{V} we need to solve the multi dimensional integral over position, p , and momentum, q :

$$\mathcal{V} = \frac{\int d^{3N}p d^{3N}q \mathcal{V}(p, q) e^{-E/k_B T}}{\int d^{3N}p d^{3N}q e^{-E/k_B T}}, \quad (5.2)$$

i.e., we need to integrate over all configurations that are consistent with the constraints applied to it. Here the integration over momentum space can be carried out separately. These integrals are impossible to solve for anything but the most simple systems and approximative methods must therefore be used. The ordinary Monte Carlo algorithm is an approach to solve these problems by random sampling of the integrand. In this case we would thus generate a set of random configurations and calculating the approximate value $\overline{\mathcal{V}}$ of eq. 5.2 as

$$\mathcal{V} \approx \overline{\mathcal{V}} = \frac{\sum_i \mathcal{V}_i e^{-E_i/k_B T}}{\sum_i e^{-E_i/k_B T}} \quad (5.3)$$

While this method of integration can produce good estimations if the integrand varies slowly over its domain, this is not the case here since the energy landscape of the configuration space of densely packed matter usually have few very sharp minima dispersed in a large $3N$ dimensional space of high energy states. Most randomly picked configurations will thus be high energy states of very low probability, and finding the probable low energy states by chance is a numerical search for the notorious needle in the haystack. To make sure that some low energy states are included in the sum of eq. 5.3 and a very large set of samples is required for an acceptable approximation.

The Metropolis Monte Carlo algorithm (MMC) (74) offers a solution to this problem. Rather than randomly sampling configurations and weighing each by its

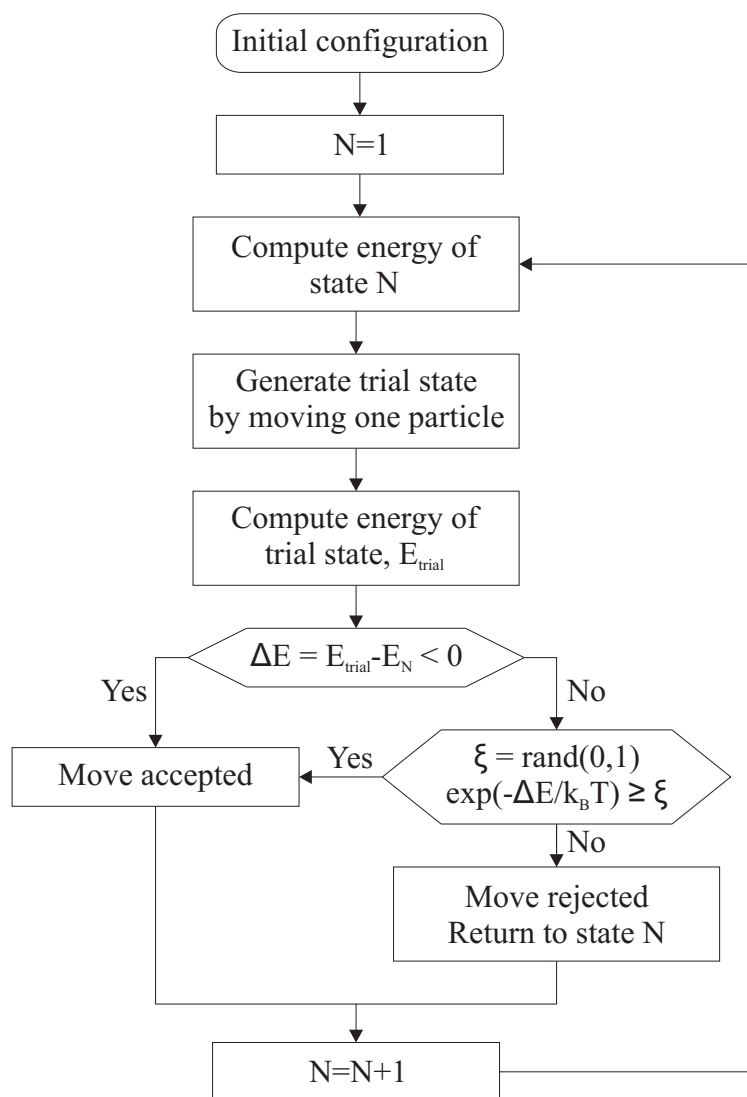


Figure 5.1: Flowchart describing the Metropolis Monte Carlo method

probability, it samples configurations with a probability of $\exp(-E/k_B T)$ and then calculate \mathcal{V} as the mean value of \mathcal{V} in these configurations. The algorithm to find configurations of $\exp(-E/k_B T)$ probability is outlined in fig. 5.1 and the steps are further described here. If we start at some configuration labeled n , we create a trial configuration by moving one particle, located at \mathbf{r}_i , in a random direction;

$$\mathbf{r}_{trial} = \mathbf{r}_i + a\boldsymbol{\zeta}, \quad (5.4)$$

where $a\boldsymbol{\zeta}$ is a random vector such that $|a\boldsymbol{\zeta}| \leq a$, and calculate the change in energy of the system $\Delta E = E_{trial} - E_0$. If $\Delta E \leq 0$, the move is accepted and if not, it is accepted with the probability $\exp(-\Delta E/k_B T)$. If the move is not accepted, the system is returned to its previous state. We label this new state (also a rejected move results in a 'new' state) as $n + 1$ and continue to move another particle randomly. After M steps we have generated a so called Markov chain of M configurations, distributed according to the Boltzmann distribution. Given enough iterations we can (as all moves, and thereby configurations, have a finite probability) move through the entire configuration space. From this set of M states the MMC approximation of observable \mathcal{V} is the sum over all M selected states:

$$\mathcal{V} \approx \overline{\mathcal{V}} = \frac{1}{M} \sum_{i=1}^M \mathcal{V}_i, \quad (5.5a)$$

and

$$\lim_{M \rightarrow \infty} (\overline{\mathcal{V}} - \mathcal{V}) = 0. \quad (5.5b)$$

As in molecular dynamics, the start configuration is rarely a low energy state and may thus skew the Boltzmann distribution, so before we start collecting configurations the system should be allowed to equilibrate properly during a number of iterations until the memory of its start position has been lost.

MMC is less computationally expensive than an MD simulation of the same system, but will on the other hand only generate static structural information. It also shares some of the problems of MD, such as the same problem of finding realistic interaction potentials. The potentials used are obtained in a way similar to those of MD simulations, and as in MD, developments of QM incorporations to calculate the electronic interactions have been made.

5.1.3 Reverse Monte Carlo

For both MD and MMC simulations there is only one way to tell if the chosen potentials are good enough approximations of the true interactions, and that is to compare calculated observables, such as nearest neighbor distances and pair correlation functions, with the corresponding experimental data. If the computed and experimental quantities do not agree, new interaction potentials must be chosen and the calculations redone. An alternative route towards a construction of a structure model would

be to directly produce a model that agrees with experimental data, which is exactly what the reverse Monte Carlo (RMC) method does.

The RMC algorithm (75; 76; 77) is a variation of the MMC algorithm, with the difference that the energy of the system has been replaced by a parameter χ that describes the difference between experimental values and the corresponding quantities calculated from the structure model. For x-ray or neutron diffraction data, the parameter χ_n^2 for the n^{th} model takes the form

$$\chi_n^2 = \sum_{i=1}^m \frac{(S_n^C(Q_i) - S^E(Q_i))^2}{\sigma_i^2(Q_i)}, \quad (5.6)$$

where $S_n^C(Q_i)$ and $S^E(Q_i)$ are the computed and experimental structure factors at wave vector Q_i (at m discrete points) and $\sigma_i^2(Q_i)$ relates to the experimental errors at that wave vector. The algorithm is outlined in figure 5.2 and is, as can be seen, similar to the MMC algorithm.

Starting from some initial configuration ($n=0$), the total structure factor and χ_n^2 are calculated. One particle is moved at random as in the MMC, eq. 5.4, and χ_{trial}^2 is calculated for the new configuration. If $\chi_n^2 - \chi_{\text{trial}}^2 \geq 0$ the move is accepted and else it is accepted with the probability $\exp(-(\chi_n^2 - \chi_{\text{trial}}^2)/2)$. The new configuration is labeled $n+1$ and a new iteration begins (now comparing the trial configuration to configuration $n+1$).

Comparing this to the MMC method we see that the driving force of RMC is χ^2 where MMC uses energy, and that the experimental errors in RMC correspond to the temperature in MMC. This comparison is correct on an analysis of the algorithm, but physically this similarity is not important. The exact form of χ^2 is chosen simply because it works. The important part of RMC is the possibility for a move to be accepted despite that it increases the deviation from the experimental data. This ensures that the entire configurational space may (just as in MMC) be investigated, given that a large enough number of moves are made.

A key feature of RMC is the ability to obtain a configuration that is in quantitative agreement with several sets of data. The only requirement is that the corresponding quantity can be calculated from the static structural model that RMC produces. Given a set of experimental data on the form $D_j^E(X_{j,i})$ which allow a computation of a corresponding $\chi_{j,n}^2$, the total deviation χ_n^2 may be calculated as

$$\chi_n^2 = \sum_{j=1}^N \chi_{j,n}^2 \quad (5.7)$$

Thus, one may use several data sets that do not need to be defined on the same domain, or even dimension (e.g. simultaneously fitting both structure factors (dimension \AA^{-1}) and real space correlations (\AA)).

In addition to minimize the deviation to diffraction data, several types of constraints on the structure, based on other experimental techniques or chemical knowledge, may be incorporated into the RMC model. The most common constraint is

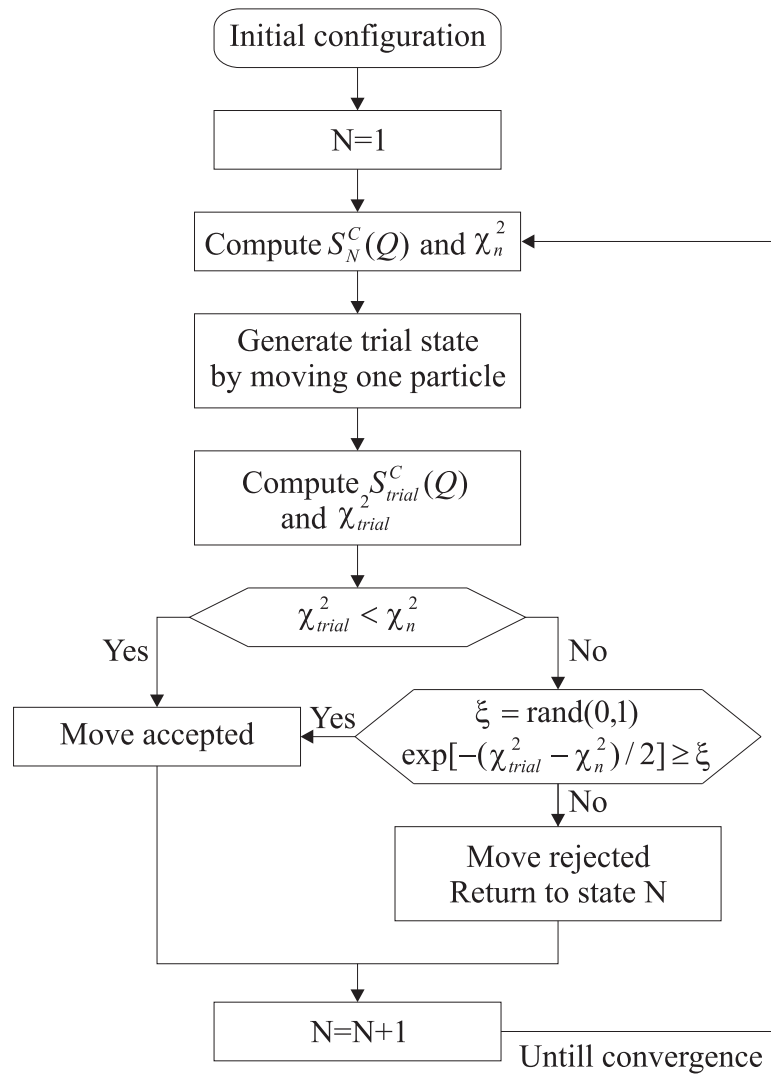


Figure 5.2: Flow chart of the reverse Monte Carlo algorithm.

the minimum nearest neighbor distance, realized by rejecting moves that places any two atoms too close to each other. In materials with well defined SRO, such as the network glasses described earlier or molecular liquids, the knowledge of coordination numbers from e.g. EXAFS or NMR measurements may be included. If we define the proportion of atoms in the modeled structure of type a that has a given coordination to atoms of type b as f_{ab}^{RMC} and the required proportion as f_{ab}^{req} then

$$\chi_n^2 = \sum_{a,b} \chi_{ab,n}^2 = \sum_{a,b} \frac{(f_{ab}^{RMC} - f_{ab}^{req})^2}{\sigma_{ab}^2}. \quad (5.8)$$

σ_{ab}^2 here acts as the weight of the $a - b$ coordination constraint compared to other experimental χ^2 . Bond valence constraints can likewise be included in the modeling to further improve the local bond lengths. Throughout our RMC calculations, we have included BV constraints by adding the term

$$\chi_{BV,n}^2 = \sum_i \frac{\Delta V_i^2}{\sigma_{BV,i}^2}, \quad (5.9)$$

where ΔV_i is the bond valence mismatch of ion i (see section 5.2 for details on the BV method). Other forms of BV constraints exist, see e.g., the implementation in `RMCPow` (78; 79).

The main advantage of RMC is, as has already been mentioned, that it will produce a model of the structure that is consistent with experimental data (provided that they do not contain any systematic errors) without the need for any interaction potential. It is also computationally efficient since the calculation time for each step is of the order N , the number of atoms in the model, whereas MD simulations are of the order N^2 . RMC can thus produce larger models using less computing resources. The lack of potentials in RMC will however mean that the structure model produced is not necessarily minimized with respect to energy and as in MMC, there is no dynamical information in the model. Furthermore, since potentials often are transferable between different systems, MD and MMC allow modeling of entirely new materials, whereas RMC requires that a real sample has been produced and the relevant measurements have been performed.

The RMC method is under constant improvement and new implementations for special applications as well as novel uses of RMC has been developed. On the software side there is the original RMC program: `RMCA`, currently in version 3.14. It has two direct extensions in `RMCPow` (78; 79) and `RMCProfile` (80), both geared towards structural determinations of crystalline materials, although they should be able to handle amorphous materials as well. `RMC++` (81) is a rewrite of the original `RMCA` in C++ and is, like its predecessor, written primarily for amorphous material modeling. All these can be found through the `ISIS RMC` page (82).

The RMC algorithm has also been developed to include dynamics data, such as the dynamic structure factor, $S(Q, \omega)$ from inelastic or quasi elastic neutron diffraction scattering or IR vibrational spectroscopy. The `RMCT` (83) algorithm works with a set of structure models where each model represents a single time step. Each of

these time steps should fit well to the static part of the experimental data (and constraint) as in the ordinary RMC method, but the ensemble as such should additionally fit the dynamics data. At this time a satisfactory reproduction of quasi-experimental data, calculated from MD simulations, have been reported (83).

5.2 The Bond Valence Method

In 1929 L. Pauling published five rules for the structure of inorganic compounds, particularly crystalline systems (84). The second of these rules was;

In a stable coördination structure the electric charge of each anion tends to compensate the strength of the electrostatic valence bonds reaching to it from the cations at the centers of the polyhedra of which it forms a corner; that is, for each anion

$$\zeta = \sum_i \frac{z_i}{v_i} = \sum_i s_i.$$

ζ , z_i and v_i are defined such that, if e is the electronic charge then; $-e\zeta$ is the charge of the anion, ez_i is the charge of cation i , v_i its coordination number and s_i is the strength of the electrostatic valence bond going from the cation to each of the surrounding anions. In short, this rule tells us that the electric charge of an anion in a stable compound should be locally balanced by the positive charge of the surrounding cations to which it is coordinated. The strength of the bond is here defined only as the electronic charge of the anion divided by its coordination number.

Donnay and Allman (85) generalized the Pauling rule to include the relation between the length of a bond and its strength by expressing the valence as $\zeta = \sum_i s(R)_i$. To avoid confusion this new expression was renamed *bond valence* (BV). Various forms for the bond valence exist but the most commonly used form is the exponential form suggested by Brown and Altermatt (86)

$$S_{M-X} = e^{\frac{R-R_0}{b}}, \quad (5.10)$$

where R_0 and b are bond valence parameters. R_0 is the unit valence distance and is related, but not equal to the ideal bond length. b on the other hand is related to the softness of the bond, which will be discussed later. The total valence of an ion M is then the sum of individual bond valence contributions from each ligand it is coordinated to:

$$V_M = \sum_X S_{M-X}. \quad (5.11)$$

This expression can easily be extended to include more than one type of ligand atoms by summation over all types

$$V_M = \sum_i \sum_{X_i} S_{M-X_i} = \sum_i \sum_{X_i} e^{\frac{R_{X_i}-R_{0,i}}{b_i}}, \quad (5.12)$$

where X_i is ligand atoms of type i .

In a stable coordination environment, V_M should be close to the formal charge (the oxidation state) of M . The bond valence parameters R_0 and b can then be calculated from sets of refined crystalline structures containing $M - X$ coordinations where the two parameters are optimized such that the bond valence sum of each atom is as close to the ideal valence as possible. Commonly, only the nearest neighbors (i.e. ions in the first coordination shell) are considered to contribute to the bond valence sum. However, due to the limited range of bond lengths and varying coordination environments in crystalline structures, an independent refinement of both R_0 and b is difficult to achieve for many atom pairs, and thus a universal value of $b = 0.37$ is commonly used (86). With a refined value for R_0 , most atoms in their equilibrium position in a crystalline structure have a valence deviation from their ideal value (a bond valence mismatch $\Delta V = |V - V_{ideal}|$) of less than 0.05 valence units (v.u.). This rather narrow expected mismatch of crystalline equilibrium sites is used as a standard tool in crystallography to evaluate the plausibility of proposed crystalline structures. A calculation of the root mean square of ΔV_O for all atoms yields the *global instability index*, which at high values (> 0.2 v.u.) indicates probable instability of the structure and can therefore be considered unlikely (87; 88; 89).

BV is also a valuable tool for locating light elements such as H and Li in structures derived from X-ray diffraction data. The original proposal of the Donnay and Allman paper was indeed to use bond valence as a tool to distinguish O^{-2} , OH^{-1} and H_2O from each other in crystalline structures. If the total valence contribution to an oxygen from the known (i.e. not hydrogens) cations in the structure is calculated, the mismatch of its total valence can only be reduced by the presence of hydrogen atoms. In this way, the valence mismatch indicates how many hydrogens it must bind to, for its valence to be close to the ideal 2 v.u.

A more general method for localization of equilibrium positions of atoms in a proposed structure was presented by Waltersson (90) where he shows that the Li positions in a range of crystals can be accurately predicted by calculating the total valence of a hypothetical Li placed at several position in the unit cell, thereby creating a 3d map of the valence landscape. Asserting that the most probable equilibrium sites are those where $\Delta V \approx 0$ he could then identify the same Li sites as those found by experimental techniques. Similar use of BV calculations are used to locate ions in protein structures (91).

The traditional bond valence approach of including only the first coordination shell is usually sufficient if one is interested in the valence of an ion in a highly symmetrical coordination polyhedron, but in distorted structures this first coordination shell can be difficult to define or may even be a meaningless concept. By instead performing the sum in equation 5.12 over all atoms within a cut-off radius, R_{co} , which covers more than the first coordination shell, this problem may be avoided. Furthermore, using a larger radius will include more atomic distances in parameter refinement and thus make an independent refinement of both R_0 and b possible. Brown and Altermatt (86) chose $R_{cut-off} = 2.67\text{\AA}$ but a later study by Adams (92) revealed the importance of considering how the choice of $R_{cut-off}$ affected the least

square fit of R_0 and b . For most ion pairs, the cut-off distance in the *soft-BV* parameter set of Adams lies between 5 and 8 Å. Increasing the distance over which surrounding ions may contribute to the valence of a central ion also means that BV-maps now takes the form of a smooth function, resembling an energy landscape, rather than the discontinuous nature it takes if $R_{cut-off}$ is too short.

Despite the increased cut-off radius, the lack of sufficiently many reliable crystalline structures still pose a problem in finding proper values of b for many of the less common atomic pairs. While this pose little problem in the refinement of crystalline structures, a proper b value is important in modeling the different bond softness between different ionic pairs when, e.g., disordered systems are studied. Additionally, treating b as a strictly empirical parameter also prevents any meaningful theoretical treatment of the BV method. Urusov (93) have argued that the softness of the bond should increase with the sum of the softness of the interacting particles. This, however, contradicts the empirical HSAB (hard and soft acids and bases) concept (94) according to which instead suggest that reactions occur most readily between species of similar softness or hardness. Thus, Adams found that there is a relation between the difference in softness ($s_{anion} - s_{cation}$) and the value of b refined from crystalline structures. This relation not only allows an estimation of b when no crystalline data are available, but also leads to a further refinement of the structure fitted b -parameters(92; 95).

5.2.1 Bond Valence and Ionic Conductivity

Garret *et al.* introduced the idea that possible diffusion pathways of mobile ions could be determined as those regions where the valence mismatch is as low as possible. They further demonstrated the plausibility by showing the striking resemblance between the isosurfaces of $V_{Ag}^{-\gamma}$, ($\gamma > 0$), and a neutron diffraction difference map, showing the Ag density in a α -AgI unit cell. A 3d representation of these BV-pathways is shown in fig. 5.3 and shows a strong similarity to the Ag densities calculated by first-principles MD (34). A direct comparison of Ag pathways in the superionic $RbAg_4I_5$ determined experimentally and by bond valence calculation is shown in figure 5.4

The work of Adams (92), mentioned in the previous section, did not only investigate how $R_{cut-off}$ should be chosen, but looked into all aspects of how the bond valence parameters need to be defined in highly asymmetrical positions, such as those common in amorphous materials. The extension of the cut-of radii meant that the refinement of R_0 and b now could be done over far more M–X pairs in the crystalline structures, thereby allowing a refinement of both parameters.

A calculation of the bond valence pathways do not only yield a description of their diffusion, but can also be used to determine the activation energy of diffusion. If the BV landscape is related to the energy landscape, there should be a relation between the lowest BV mismatch for which a percolating pathway is formed and the activation energy, if E_a is determined by energy bottlenecks that the ion must be able to pass. In crystalline solids, this relation has been found to exist for a set of

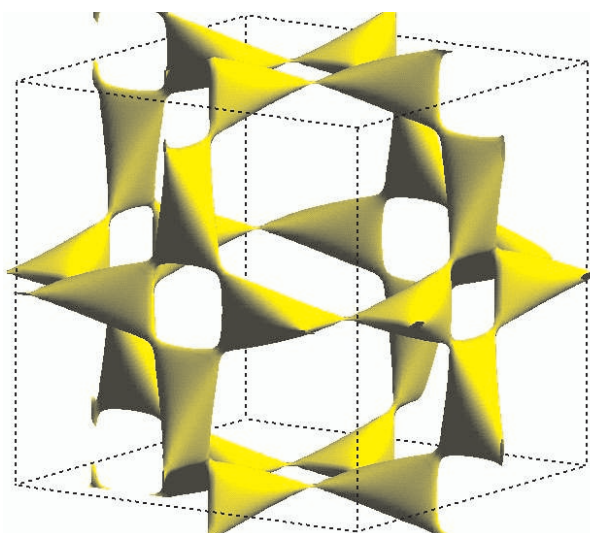


Figure 5.3: Pathways of Ag conduction in the crystalline α -AgI. Iodine ions arranged in a body centered cubic lattice (not shown) are located in the corners of the unit cell and in its center, while Ag can move in the BV region. From (96)

Ag-conducting vanadium oxide, tungstate and phosphate crystals (97). Application to glass systems, modeled by RMC, soon followed in which Adams and Swenson showed that the BV method is applicable to highly disordered systems as well (98; 99; 100).

Calculation of BV Landscape and Pathways

The calculation of the bond valence landscape used in our investigations are similar to the approach by Waltersson and later Garret, and is here presented in some detail.

The bond valence landscape in an RMC produced structural model is calculated by dividing the model volume into ca 4 million cubic sub-volumes, wherein the total bond valence of a hypothetical mobile ion in its center is calculated. Volume elements whose valence mismatch, ΔV is less than a chosen maximum mismatch ΔV_{max} , and are not within the nearest neighbor distance of any immobile ions, are said to be accessible for the mobile ion. A set of accessible volume elements that are edge or face sharing are said to belong to a cluster, within which a mobile ion can move. A cluster that form an infinite, percolating cluster through the periodic model volume is thus a pathway for dc conductivity. A finite cluster on the other hand can not participate in dc conduction, but may very well take part in ac conductivity, provided that the frequency is high enough* that the ions in average travel a shorter distance than the size of the cluster. The percolating cluster is here denoted \mathcal{P} , and the fractional volume it occupies in the model is denoted as $\mathcal{F}(\mathcal{P})$

*High in relation to the electric field, mobile ion mass, etc.

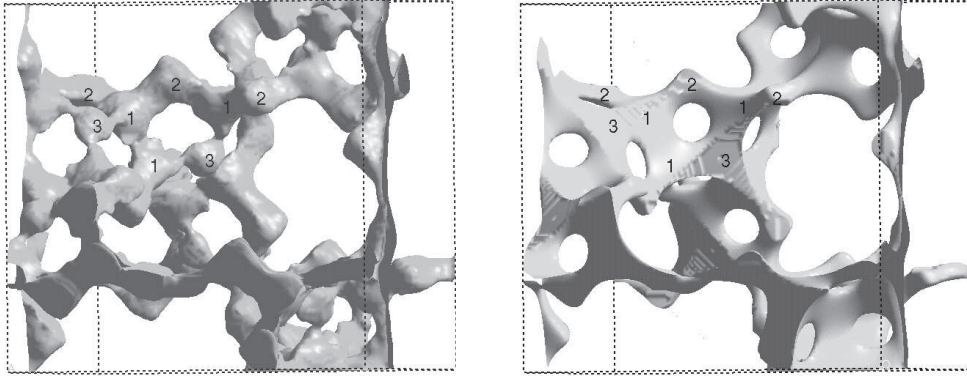


Figure 5.4: Comparison of experimentally determined Ag density in RbAg_4I_5 (left) and the pathways predicted from the bond valence method (96)

Ionic Conductivity in Glasses

The BV pathways can provide plenty of information on the ionic conduction process in a glass. While an estimation of E_a in principle should be possible to do by determining the lowest ΔV_{max} for which a percolating cluster forms as in crystalline structures, but it has proven difficult to determine this valence mismatch value in amorphous material with a sufficient confidence. Instead a relation between the fractional volume and both activation energy and dc conductivity (95; 101) according to

$$\log(\sigma T \sqrt{(m)}) = A + B \sqrt[3]{\mathcal{F}} \quad (5.13a)$$

$$-\frac{E_a}{k_b T} = A' + B' \sqrt[3]{\mathcal{F}} \quad (5.13b)$$

\mathcal{F} is here calculated for the arbitrary value of $\Delta V_{max} = 0.2 \text{ v.u.}$ While this choice may seem critical, it has been shown that there is no large variation in the results of equations 5.13 between different glasses, nor mobile ions, as long as ΔV_{max} is kept reasonably low, commonly 0.1-0.3 v.u.

CHAPTER 6

Summary of Appended Papers

Paper I

THE NATURE OF CONDUCTION PATHWAYS IN MIXED ALKALI PHOSPHATE GLASSES

$\text{Li}_x\text{Rb}_{1-x}\text{PO}_3$ glasses show a strong mixed alkali effect at room temperature. At an intermediate composition ($x = 0.5$) the conductivity is 7 orders of magnitude below that of either of the pure glasses. In this paper we investigate the nature of the conduction pathways in these glasses by means of bond-valence analysis, starting from static structural models. It is shown that the pathways have a relatively low dimensionality at distances $< 4 \text{ \AA}$, and since the ions are randomly distributed the blocking of pathways is very effective. It is also shown that the most local neighborhood ($< 0.7 \text{ \AA}$) of a site in the pathway of ion A do not change significantly when ions of type B is introduced into the glass.

Paper II

LOCAL DIMENSIONALITY AND INTERMEDIATE RANGE ORDERING OF ION CONDUCTION PATHWAYS IN BORATE GLASSES.

When silver, lithium and sodium di-borate glasses are doped by metal halide salts (AgI, NaCl and LiCl), a similar increase in conductivity occurs in all three systems. Earlier studies of RMC modeled structures from neutron and X-ray diffraction data have revealed that although all three glasses have very similar SRO in the boron network, their intermediate-range structure is highly dependant on the type of mobile ion. These differences are in particularly large for the highly doped glasses, where AgI is homogeneously introduced in the glass, causing an expansion of the borate network, whereas LiCl and NaCl are more inhomogeneously distributed, forming microscopic clusters of salt ions.

The ionic pathways of these RMC models were calculated using the bond-valence

method and their topography is compared to that of the glass structure. It is shown that the Ag pathways have correlations similar to that of the borate network, indicating that the Ag ions are moving in channels adjacent to the borate network in both the undoped and doped glasses. In the LiCl and NaCl glasses a direct comparison of correlations were not as relevant due to the lack of well defined intermediate range order in the highly doped glasses, whereas some similarities between borate network correlations and pathway correlations could be seen in the undoped glasses. The large differences seen for both atomic structure and pathways in the three glass systems indicate that the intermediate range order does not play a direct role in ionic conductivity in these systems

Paper III

COMPARATIVE STUDY OF ION CONDUCTING PATHWAYS IN BORATE GLASSES

Here we extend our study of the di-borate glasses in paper II. The two main additions in this paper is; a) Importance of oxygen coordination in the pathway and b) the importance of the intermediate range order.

The importance of oxygen coordination in highly doped glasses has been a matter of debate. It has been argued that the mobile ions are mainly coordinated to halide ions, providing them with fast conduction pathways similar to those in the corresponding FIC crystals, and that slow, oxygen coordinated bridges connect these regions. Here we show that the mobile ions have a relatively high preference for mixed oxygen/halide coordination.

The hypothesis that the relatively well defined order in AgI doped di-borate glass contributes to its high ionic conductivity was tested by generating a set of more or less random glass models. In the AgI doped glass, the volume of the ionic pathways is not significantly changed as long as the borons and oxygens are coordinated in a network structure. In LiCl and NaCl doped di-borates, a pronounced drop in pathway volume was seen in the random structures. Our conclusion from these findings is that the high conductivity of AgI doped glasses is primarily an effect of the local environment of the mobile ion, and not the unusually ordered intermediate-range structure.

Paper IV

STRUCTURE OF $Ag_xNa_{(1-x)}PO_3$ GLASSES BY NEUTRON DIFFRACTION AND REVERSE MONTE CARLO MODELLING

The mixed Ag/Na metaphosphate glass system shows an interesting low mixed mobile ion effect in its ionic conductivity. The variation of dc-conductivity with Ag to Na exchange is close to linear, though a minimum, ca 0.5 decades under σ_{dc} of the single Na glass is clear at 75 % Na content. An investigation of this system and a comparison of our findings with those from the mixed Li/Rb metaphosphate system earlier studied (in paper 1 and refs. (102; 60)) can thus provide us with important insight into the MMIE. $Ag_xNa_{1-x}PO_3$ glasses of compositions $x=\{1, 0.75,$

0.5, 0.25,0} were measured by neutron and X-ray diffraction, whereafter structure models of all compositions were created using reverse Monte Carlo modeling with bond valence constraints. We found that, unlike the mixed Li/Rb system, there are almost no changes in the structure when Na replaces Ag in the glass. The two mobile ions show a preference to similar sites in the glass network. Our conclusion of this study is that there is a low energy mismatch for an Ag ion to hop into an Na site and vice versa and that the two ions can share pathways without blocking each others movement.

Paper V

MIXED MOBILE ION EFFECT AND COOPERATIVE MOTIONS IN SILVER-SODIUM PHOSPHATE GLASSES

We continue our study of the $\text{Ag}_x\text{Na}_{1-x}\text{PO}_3$ glass system from paper IV by calculating the pathways of Ag and Na ion using the bond valence method. We find that the structural changes are negligible also from the perspective of the ionic pathways, although a slight increase in their volume occurs (for both Ag and Na pathways) at the Ag-richer compositions. Furthermore, the two ions share pathways to a large extent and can thus participate in the same conduction mechanism. If the weak MMIE we do see in the system originates in the same blocking effect as earlier described for the Li/Rb metaphosphate system, it can only involve a very small subset of the unlike ions. In this article we also propose that the weak non-linearity could be due to a dynamic effect, due to the very different masses of the ions.

Paper VI

STRUCTURE OF $\text{Li}_x\text{Rb}_{1-x}\text{PO}_3$ GLASSES NEAR THE GLASS TRANSITION

While a wide range of glasses follow an Arrhenius behavior of the dc-conductivity below T_g , a deviation from this can be seen as the temperature is raised above it. In this paper, we have studied the temperature dependence of the glass structure in the mixed Li/Rb metaphosphate system, from room temperature up to 10-30 K above the glass temperature. We find that there is no significant changes of the PO-network throughout this temperature range and calculations of the bond valence pathways reveal that the adaptation of the glass to the mobile ion show no significant change either. Any deviation from Arrhenius behavior is proposed to be caused by increased network dynamics akin to the dynamic structure model.

My contribution to the papers

In all papers I have been responsible for writing the manuscript and produced most figures. Additionally, I have performed all bond valence calculations and the subsequent analysis of the pathways using software written by me in C++ and Matlab.

In papers IV-VI I have additionally prepared glass samples for neutron and X-ray diffraction, taken part in the neutron diffraction experiments at ISIS, corrected both

neutron and X-ray data and modeled the glass structures using RMCA.

Discussions with Stefan Adams (papers I–III, V) and Jan Swenson (I–VI) have contributed substantially to the final content of the papers.

Acknowledgments

First of all, I would like to thank my supervisor, Jan Swenson, for your support and guidance through the world of science, for all the language corrections of my notoriously bad English grammar and of course your apparently infinite patience for not giving up on me completely.

Close second is Stefan Adams. Your hospitality towards me during my stays in Germany and of course all invaluable discussions on bond valence. I can't imagine this work being completed without it.

Daniel Bowron and Carlo Meneghini for patiently trying to guide me through the secrets of diffraction data correction.

Lars Börjesson and Per Jacobsson, the bosses of each other, and me, for arranging this clear, hierarchic leadership and managing to get both group and department to run so smoothly.

The members, past and present, of the Condensed Matter Physics group for the environment in which I've spent the last six years. In particular my "sambos", Helen and Peter for non-physics related talks in times of desperate need and desperate boredom. Oh, and whoever has been buying the coffee all this time!

Friends. I still have some, to my amazement. Thank you for still hanging around

And last, but certainly not least: My family.

I wouldn't be standing here, had it not been for what my mother have done for me, and what the rest of my family would have done.

And for all the years before that as well.

Bibliography

- [1] P. A. Bland, C. R. De Souza Filho, A. J. T. Jull, S. P. Kelley, R. M. Hough, N. A. Artemieva, E. Pierazzo, J. Coniglio, L. Pinotti, V. Evers, and A. T. Kearsley, *A possible tektite strewn field in the Argentinian Pampa*, *Science* **296**, 1109 (2002).
- [2] G. R. Osinski, H. P. Schwarcz, J. R. Smith, M. R. Kleindienst, A. F. C. Haldermann, and C. S. Churcher, *Evidence for a ? 200-100Â ka meteorite impact in the Western Desert of Egypt*, *Earth and Planetary Science Letters* **253**, 378 (2007).
- [3] J. J. Disa, J. Vossoughi, and N. H. Goldberg, *A COMPARISON OF OBSIDIAN AND SURGICAL STEEL SCALPEL WOUND-HEALING IN RATS*, *Plastic and Reconstructive Surgery* **92**, 884 (1993).
- [4] M. J. Scott, *OBSIDIAN SURGICAL BLADES - MODERN USE OF A STONE-AGE IMPLEMENT*, *Journal of Dermatologic Surgery and Oncology* **8**, 1050 (1982).
- [5] W. H. Zachariasen, *Atomic arrangement in glass*, *Ceramic Industry* **20**, 269 (1933).
- [6] S. R. Elliott, *Physics of amorphous materials (second edition)*, 2nd ed. (Longman Scientific & Technical, Essex, 1990).
- [7] H. E. Stanley, *Unsolved mysteries of water in its liquid and glass states*, *MRS Bulletin* **24**, 22 (1999).
- [8] P. J. Collings and M. Hird, *Introduction to Liquid Crystals* (Taylor & Francis, London, 1997).
- [9] L. Pusztai and O. Gereben, *On the determination of the structure of metallic glasses by reverse Monte Carlo simulation: comparison with hard sphere*

- Monte Carlo results*, Materials Science and Engineering A **179-80**, 433 (1994).
- [10] G. N. Greaves, *EXAFS and the structure of glass*, Journal of Non-Crystalline Solids **71**, 203 (1985).
- [11] J. Swenson, L. Börjesson, and W. S. Howells, *Structure of borate glasses from neutron-diffraction experiments*, Physical Review B **52**, 9310 (1995).
- [12] J. Swenson, L. Börjesson, and W. S. Howells, *Structure of fast-ion-conducting lithium and sodium borate glasses by neutron diffraction and reverse Monte Carlo simulations*, Physical Review B **57**, 13514 (1998).
- [13] A. N. Cormack, X. Yuan, and B. Park, in *Molecular dynamics simulations of silicate glasses and melts*, Vol. 27 of *Glass Phys. Chem. (Russia)* (MAIK Nauka, St. Petersburg, Russia, 2001), pp. 28–36.
- [14] J. J. Hudgens and S. W. Martin, *Glass transition and infrared spectra of low-alkali, anhydrous lithium phosphate glasses*, Journal of the American Ceramic Society **76**, 1691 (1993).
- [15] R. K. Brow, *Review: the structure of simple phosphate glasses*, Journal of Non-Crystalline Solids **263**, 1 (2000).
- [16] E. Chason and F. Spaepen, *Pressure-induced structural changes in boron oxide glass*, Journal of Applied Physics **64**, 4435 (1988).
- [17] J. Swenson and L. Börjesson, *Fraction of boroxol rings in vitreous boron trioxide*, Physical Review B **55**, 11138 (1997).
- [18] G. Ferlat, T. Charpentier, A. P. Seitsonen, A. Takada, M. Lazzeri, L. Cormier, G. Calas, and F. Mauri, *Boroxol rings in liquid and vitreous B₂O₃ from first principles*, Physical Review Letters **101**, (2008).
- [19] J. Swenson and L. Börjesson, *Comment on "fraction of boroxol rings in vitreous boron oxide from a first-principles analysis of Raman and NMR spectra"*, Physical Review Letters **96**, (2006).
- [20] E. Kashchieva, B. Shivachev, and Y. Dimitriev, *Molecular dynamics studies of vitreous boron oxide*, Journal of Non-Crystalline Solids **351**, 1158 (2005).
- [21] D. R. Uhlmann and R. R. Shaw, *The thermal expansion of alkali borate glasses and the boric oxide anomaly*, Journal of Non-Crystalline Solids **1**, 347 (1969).
- [22] G. Chiodelli, A. Magistris, M. Villa, and J. L. Bjorkstam, *Short-Range Order and Glass-Transition in Ag₁-Ag₂O-B₂O₃ Vitreous Electrolytes*, Journal of Non-Crystalline Solids **51**, 143 (1982).

- [23] Y. H. Yun and P. J. Bray, *Nuclear magnetic resonance studies of the glasses in the system $\text{Na}_2\text{O} \cdot \text{B}_2\text{O}_3 \cdot \text{SiO}_2$* , Journal of Non-Crystalline Solids **27**, 363 (1978).
- [24] S. A. Feller, W. J. Dell, and P. J. Bray, *B-10 Nmr-Studies of Lithium Borate Glasses*, Journal of Non-Crystalline Solids **51**, 21 (1982).
- [25] E. I. Kamitsos, A. P. Patsis, M. A. Karakassides, and G. D. Chryssikos, *Infrared Reflectance Spectra of Lithium Borate Glasses*, Journal of Non-Crystalline Solids **126**, 52 (1990).
- [26] F. L. Galeener, G. Lucovsky, and J. C. Mikkelsen Jr, *Vibrational spectra and the structure of pure vitreous B_2O_3* , Physical Review B **22**, 3983 (1980).
- [27] J. Lorosch, M. Couzi, J. Pelous, R. Vacher, and A. Levasseur, *Brillouin and Raman-Scattering Study of Borate Glasses*, Journal of Non-Crystalline Solids **69**, 1 (1984).
- [28] C. P. E. Varsamis, A. Vegiri, and E. I. Kamitsos, *Molecular dynamics investigation of lithium borate glasses: Local structure and ion dynamics*, Physical Review B **65**, 104203 (2002).
- [29] A. Schiraldi, E. Pezzati, P. Baldini, and S. W. Martin, *Transport and thermodynamic properties of AgI-Ag oxysalt(s) glasses*, Solid State Ionics **18-19**, 426 (1986).
- [30] H. L. Tuller and D. P. Button, in *Transport-Structure Relations in Fast Ion and Mixed Conductors*, edited by F. W. Poulsen, N. Hessel-Anderson, K. Clausen, S. Skaarup, and O. Soerensen (Riso National Laboratory, Roskilde, 1985), p. 119.
- [31] J. Swenson and L. Börjesson, *Correlation between free volume and ionic conductivity in fast ion conducting glasses*, Physical Review Letters **77**, 3569 (1996).
- [32] W. Schottky, *Zur Theorie der thermischen Fehlordnung in Kristallen*, Die Naturwissenschaften **23**, 656 (1935).
- [33] J. Frenkel, *U?ber die Wa?rmebewegung in festen und flu?ssigen Ko?rpern*, Zeitschrift fu?r Physik **35**, 652 (1926).
- [34] B. C. Wood and N. Marzari, *Dynamical structure, bonding, and thermodynamics of the superionic sublattice in alpha-AgI*, Physical Review Letters **97**, (2006).
- [35] L. Heyne, *Some aspects of solid electrolytes*, Electrochimica Acta **15**, 1251 (1970).

- [36] B. B. Owens and G. R. Argue, *High-conductivity solid electrolytes: MAg4I5*, *Science* **157**, 308 (1967).
- [37] J. N. Bradley and P. D. Greene, *Solids with high ionic conductivity in group I halide systems*, *Transactions of the Faraday Society* **63**, 424 (1967).
- [38] M. D. Ingram, *IONIC-CONDUCTIVITY IN GLASS*, *Physics and Chemistry of Glasses* **28**, 215 (1987).
- [39] M. D. Ingram, M. A. Mackenzie, W. Muller, and M. Torge, *CLUSTER AND PATHWAYS - A NEW APPROACH TO ION MIGRATION IN GLASS*, *Solid State Ionics* **28**, 677 (1988).
- [40] O. L. Anderson and D. A. Stuart, *Calculation of activation energy of ionic conductivity in silica glasses by classical methods*, *American Ceramic Society – Journal* **37**, 573 (1954).
- [41] D. Ravaine and J. L. Souquet, *Thermodynamic Approach to Ionic-Conductivity in Oxide Glasses .1. Correlation of Ionic-Conductivity with Chemical Potential of Alkali Oxide in Oxide Glasses*, *Physics and Chemistry of Glasses* **18**, 27 (1977).
- [42] P. Maass, A. Bunde, and M. D. Ingram, *Ion transport anomalies in glasses*, *Physical Review Letters* **68**, 3064 (1992).
- [43] A. Bunde, M. D. Ingram, and P. Maass, *Dynamic structure model for ion transport in glasses*, *Journal of Non-Crystalline Solids* **172-7**, 1222 (1994).
- [44] A. Bunde, M. D. Ingram, and S. Russ, *A new interpretation of the dynamic structure model of ion transport in molten and solid glasses*, *Physical Chemistry Chemical Physics* **6**, 3663 (2004).
- [45] P. Maass, *Towards a theory for the mixed alkali effect in glasses*, *Journal of Non-Crystalline Solids* **255**, 35 (1999).
- [46] C. A. Angell, *Recent developments in fast ion transport in glassy and amorphous materials*, *Solid State Ionics* **18-19**, 72 (1986).
- [47] K. Funke, *Jump relaxation in solid electrolytes*, *Progress in Solid State Chemistry* **22**, 111 (1993).
- [48] K. Funke, *Jump relaxation model and coupling model - a comparison*, *Journal of Non-Crystalline Solids* **172-174**, 1215 (1994).
- [49] D. E. Day, *Mixed alkali glasses – Their properties and uses*, *Journal of Non-Crystalline Solids* **21**, 343 (1976).
- [50] J. O. Isard, *The mixed alkali effect in glass*, *Journal of Non-Crystalline Solids* **1**, 235 (1969).

- [51] G. B. Rouse, P. J. Miller, and W. M. Risen, *Mixed Alkali Glass Spectra and Structure*, Journal of Non-Crystalline Solids **28**, 193 (1978).
- [52] D. E. Day, *Structural role of nitrogen in phosphate glasses*, Journal of Non-Crystalline Solids **112**, 7 (1989).
- [53] S. C. WATERTON and W. E. S. TURNER, *Some Properties of Mixed Alkali-Lime-Silica, Glasses containing Lithia, Soda, Potash and Rubidia.*, Journal of the Society of Glass Technology **18**, 268 (1934).
- [54] F. C. Baumann, J. P. Harrison, R. O. Pohl, and W. D. Seward, *Thermal conductivity in mixed alkali halides: KCl:Li and KBr:Li*, Physical Review **159**, 691 (1967).
- [55] M. Maly-Schreiber, P. Linhardt, and M. W. Breiter, *CHARACTERISATION AND PROPERTIES OF MIXED (Ag, Na) POLYCRYSTALLINE BETA double prime -ALUMINAS*, Solid State Ionics **23**, 131 (1987).
- [56] T. Uchino, T. Sakka, Y. Ogata, and M. Iwasaki, *A new model of ionic transport for single- and mixed-alkali oxide glasses based on ab initio molecular orbital calculations*, Journal of Non-Crystalline Solids **146**, 26 (1992).
- [57] J. Habasaki, K. L. Ngai, and Y. Hiwatari, *"Cooperativity blockage" in the mixed alkali effect as revealed by molecular-dynamics simulations of alkali metasilicate glass*, Journal of Chemical Physics **121**, 925 (2004).
- [58] J. Habasaki, *On the nature of the heterogeneous dynamics of ions in ionic conducting glasses*, Journal of Non-Crystalline Solids **353**, 3956 (2007).
- [59] J. Habasaki and K. L. Ngai, *The mixed alkali effect in ionically conducting glasses revisited: A study by molecular dynamics simulation*, Physical Chemistry Chemical Physics **9**, 4673 (2007).
- [60] J. Swenson and S. Adams, *Mixed alkali effect in glasses*, Physical Review Letters **90**, 155507 (2003).
- [61] A. Hall, S. Adams, and J. Swenson, *The nature of conduction pathways in mixed alkali phosphate glasses*, Ionics **10**, 396 (2004).
- [62] M. Abou el leil, J. Heasley, and M. H. Omar, *MIXED ISOTOPE EFFECT IN LITHIUM BORATE GLASSES*, Phys Chem Glasses **19**, 37 (1978).
- [63] T. Nagasaki, R. Morishima, and T. Matsui, *Isotope effect in glass-transition temperature and ionic conductivity of lithium-borate glasses*, Journal of Nuclear Science and Technology **39**, 386 (2002).
- [64] G. B.-J. O. K. Himanshu Jain, *${}^7\text{Li}$ Nuclear Magnetic Resonance in (${}^7\text{Li}$, ${}^6\text{Li}$) and (Li, Na) Triborate Glasses*, Journal of the American Ceramic Society **68**, C (1985).

- [65] F. Henn and J. Dutour, *A microscopic flow model based on Brownian dynamics for simulating ionic diffusion in a 2D-channel geometry*, Journal of Non-Crystalline Solids **351**, 1447 (2005).
- [66] G. L. Squires, *Introduction to the theory of thermal neutron scattering*. (Dover Publications, New York, 1996).
- [67] G. E. Bacon, *X-ray and neutron diffraction* (Pergamon Press, Glasgow, 1966).
- [68] P. Jund, W. Kob, and R. Jullien, *Channel diffusion of sodium in a silicate glass*, Physical Review B - Condensed Matter and Materials Physics **64**, 1343031 (2001).
- [69] M. Vogel, *Identification of lithium sites in a model of LiPO₃ glass: Effects of the local structure and energy landscape on ionic jump dynamics*, Physical Review B **70**, (2004).
- [70] H. Lammert, M. Kunow, and A. Heuer, *Complete identification of alkali sites in ion conducting lithium silicate glasses: A computer study of ion dynamics*, Physical Review Letters **90**, 2159011 (2003).
- [71] P. Vashishta, R. K. Kalia, L. Wei, A. Nakano, A. Omeltchenko, K. Tsuruta, W. Jinghan, and I. Ebbsjo, *Million atom molecular dynamics simulations of materials on parallel computers*, Current Opinion in Solid State & Materials Science **1**, 853 (1996).
- [72] M. P. Allen and D. J. Tildesley, *Computer Simulation of Liquids* (PUBLISHER, Oxford, 1987).
- [73] R. Car and M. Parrinello, *Unified Approach for Molecular Dynamics and Density-Functional Theory*, Physical Review Letters **55**, 2471 (1985).
- [74] N. Metropolis, A. W. Rosenbluth, M. N. Rosenbluth, A. H. Teller, and E. Teller, *Equation of State Calculations by Fast Computing Machines*, Journal of Chemical Physics **21**, 1087 (1953).
- [75] R. L. McGreevy and L. Pusztai, *Reverse Monte Carlo Simulation: A New Technique for the Determination of Disordered Structures*, Molecular Simulation **1**, 359 (1988).
- [76] R. L. McGreevy, *RMC - Progress, problems and prospects*, Nucl. Instrum. Methods Phys. Res. A **354**, 1 (1995).
- [77] R. L. McGreevy, *Reverse Monte Carlo modelling*, Journal of Physics Condensed Matter **13**, R877 (2001).
- [78] A. Mellergård and R. L. McGreevy, in *Materials Science Forum*, Vol. 378-381 of *7th European Powder Diffraction Conference*, edited by R. Delguez and E. J. Mittemeijer (PUBLISHER, Barcelona, 2001), pp. 71–76.

- [79] A. Mellergård and R. L. McGreevy, *Recent developments of the RMCPow method for structural modelling*, Chemical Physics **261**, 267 (2000).
- [80] M. G. Tucker, D. A. Keen, M. T. Dove, A. L. Goodwin, and Q. Hui, *RMCPProfile: Reverse Monte Carlo for polycrystalline materials*, Journal of Physics Condensed Matter **19**, (2007).
- [81] O. Gereben, P. Jozvári, L. Temleitner, and L. Pusztai, *A new version of the RMC++ Reverse Monte Carlo programme, aimed at investigating the structure of covalent glasses*, Journal of Optoelectronics and Advanced Materials **9**, 3021 (2007).
- [82] *Reverse Monte Carlo*, 2008.
- [83] O. Gereben, L. Pusztai, and R. L. McGreevy, *Development of the time-dependent reverse Monte Carlo simulation, RMCt*, Journal of Physics Condensed Matter **19**, (2007).
- [84] L. Pauling, *Structure of complex ionic crystals*, Journal of the American Chemical Society **51**, 1010 (1929).
- [85] G. Donnay and R. Allman, *How to Recognize O²⁻, OH⁻, and H₂O in Crystal Structures Determined by X-Rays*, American Mineralogist **55**, 1003 (1970).
- [86] I. D. Brown and D. Altermatt, *Bond-valence parameters obtained from a systematic analysis of the Inorganic Crystal Structure Database*, Acta Crystallographica **B41**, 244 (1985).
- [87] A. Salinas-Sanchez, J. L. Garcia-Munoz, J. Rodriguez-Carvajal, R. Saez-Puche, and J. L. Martinez, *Structural characterization of R₂BaCuO₅ (R=Y, Lu, Yb, Tm, Er, Ho, Dy, Gd, Eu, and Sm) oxides by X-ray and neutron diffraction*, Journal of Solid State Chemistry **100**, 201 (1992).
- [88] I. D. Brown, *The Chemical Bond in Inorganic Chemistry - the Bond Valence Model* (Oxford University Press, Oxford, 2002).
- [89] S. Adams, O. Moretzki, and E. Canadell, *Global instability index optimizations for the localization of mobile protons*, Solid State Ionics **168**, 281 (2004).
- [90] K. Waltersson, *METHOD, BASED UPON BOND-STRENGTH CALCULATIONS, FOR FINDING PROBABLE LITHIUM SITES IN CRYSTAL STRUCTURES*, Acta Crystallographica Section A **34**, 901 (1978).
- [91] P. Müller, S. Köpke, and G. M. Sheldrick, *Is the bond-valence method able to identify metal atoms in protein structures?*, Acta Crystallographica - Section D Biological Crystallography **59**, 32 (2003).

- [92] S. Adams, *Relationship between bond valence and bond softness of alkali halides and chalcogenides*, Acta Crystallographica Section B: Structural Science **57**, 278 (2001).
- [93] V. S. Urusov, *Semi-empirical groundwork of the bond-valence model*, Acta Crystallographica, Section B **51**, 641 (1995).
- [94] R. G. Pearson, *HARD AND SOFT ACIDS AND BASES*, Journal of the American Chemical Society **85**, 3533 (1963).
- [95] S. Adams and J. Swenson, *Pathway models for fast ion conductors by combination of bond valence and reverse Monte Carlo methods*, Solid State Ionics **154-155**, 151 (2002).
- [96] S. Adams, *Modelling ion conduction pathways by bond valence pseudopotential maps*, Solid State Ionics **136-137**, 1351 (2000).
- [97] S. Adams and J. Maier, *Ag migration pathways in crystalline and glassy solid electrolytes AgI-AgM_xO_y*, Solid State Ionics **105**, 67 (1998).
- [98] S. Adams and J. Swenson, *Migration pathways in Ag-based superionic glasses and crystals investigated by the bond valence method*, Physical Review B - Condensed Matter and Materials Physics **63**, 542011 (2000).
- [99] S. Adams and J. Swenson, *Determining Ionic Conductivity from Structural Models of Fast Ionic Conductors*, Physical Review Letters **84**, 4144 (2000).
- [100] J. Swenson and S. Adams, *Application of the bond valence method to reverse Monte Carlo produced structural models of superionic glasses*, Physical Review B - Condensed Matter and Materials Physics **64**, 024204 (2001).
- [101] S. Adams and J. Swenson, *Bond valence analysis of transport pathways in RMC models of fast ion conducting glasses*, Physical Chemistry Chemical Physics **4**, 3179 (2002).
- [102] C. Karlsson, A. Mandanici, A. Matic, J. Swenson, and L. Börjesson, *Ionic conductivity and the mixed alkali effect in Li_xRb_{1-x}PO₃ glasses*, Physical Review B: Condensed Matter **68**, 642021 (2003).

The Nature of Conduction Pathways in Mixed Alkali Phosphate glasses

A. Hall, S. Adams and J. Swenson

Ionics **10**, 396-404 (2004)

Local dimensionality and intermediate range ordering of ion conduction pathways in borate glasses.

A. Hall, S. Adams and J. Swenson

Journal of Non-Crystalline Solids **42-49**, 5164-5169 (2006)

Comparative study of ion conducting pathways in borate glasses

A. Hall, S. Adams and J. Swenson

Physical Review B: Condensed Matter **74**, 174205 (2006)

Structure of $\text{Ag}_x\text{Na}_{(1-x)}\text{PO}_3$ glasses by neutron diffraction and reverse Monte Carlo modelling

A. Hall, J. Swenson, S. Adams and D.T. Bowron

Journal of Physics: Condensed Matter **19**, 415115 (2007)

Mixed mobile ion effect and cooperative motions in silver-sodium phosphate glasses

A. Hall, J. Swenson, S. Adams and C. Meneghini
Physical Review Letters **101**, 19590 (2008)

Structure of $\text{Li}_x\text{Rb}_{(1-x)}\text{PO}_3$ Glasses Near the Glass Transition Temperature
A. Hall, J. Swenson, S. Adams and D.T. Bowron
(Manuscript)